Tissue microenvironment dictates the state of human induced pluripotent stem cell-derived endothelial cells of distinct developmental origin in 3D cardiac microtissues

Xu Cao[1,#], Maria Mircea[2,#], Francijna E. van den Hil[1], Hailiang Mei[3], Katrin Neumann[4], Konstantinos Anastassiadis[4], Christine L. Mummery[1], Stefan Semrau[2,*] and Valeria V. Orlova[1, *]

[1]Department of Anatomy and Embryology, Leiden University Medical Center, Einthovenweg 20, 2333ZC Leiden, The Netherlands

[2]Leiden Institute of Physics, Leiden University, 2333 RA, Leiden, The Netherlands

[3]Sequencing analysis support core, Leiden University Medical Center, Leiden, 2333ZA, The Netherlands

[4]Stem Cell Engineering, Biotechnology Center, Center for Molecular and Cellular Bioengineering, Technische Universität Dresden, 01307, Germany

#Contributed equally

*Corresponding author

ABSTRACT

Each tissue and organ in the body has its own type of vasculature. Here we demonstrate that organotypic vasculature for the heart can be recreated in a three-dimensional cardiac microtissue (MT) model composed of human induced pluripotent stem cell (hiPSC)-derived cardiomyocytes (CMs), cardiac fibroblasts (CFs) and endothelial cells (ECs). ECs in cardiac MTs upregulated expression of markers enriched in human intramyocardial ECs (iECs), such as *CD36, CLDN5, APLNR, NOTCH4, IGFBP3, ARHGAP18,* which were previously identified in the single-cell RNA-seq dataset from the human fetal heart (6.5-7 weeks post coitum). We further show that the local microenvironment largely dictates the organ-specific identity of hiPSC-derived ECs: we compared ECs of different developmental origins derived from two distinct mesoderm subtypes (cardiac and paraxial mesoderm) and found that independent of whether the ECs were cardiac or paraxial mesoderm derived, they acquired similar identities upon integration into cardiac microtissues. This was

confirmed by single-cell RNA-seq. Overall, the results indicated that whilst the initial gene profile of ECs was dictated by developmental origin, this could be modified by the local tissue environment such that the original identity was lost and the organotypic identity acquired through local environmental signals. This developmental "plasticity" in ECs has implications for multiple pathological and disease states.

INTRODUCTION

Development of the vascular system is one of the earliest events in organogenesis and defects in this process often result in embryonic and postnatal lethality. Endothelial cells (ECs) that form the inner lining of blood and lymphatic vessels are specialized cells that adapt to local microenvironmental cues to support the function of various organs. The heart is a prime example of the importance that interplay between the vasculature and the myocardium has in organ growth, remodeling, and function. ECs in the heart originate from several developmental lineages that later converge to similar states depending on their location. Structurally and functionally, ECs in the heart can be divided into the endocardium, intramyocardial capillary ECs, coronary arteries/veins and lymphatic ECs. During development, heart ECs predominantly originate in the lateral plate mesoderm that includes both pre-cardiac and cardiac mesoderm (Milgrom-Hoffman et al., 2011). Endocardium and *sinus venosus* are the two major sources on intramyocardial and coronary ECs (He and Zhou, 2018; Sharma et al., 2017a, 2017b; Tian and Zhou, 2022). Furthermore, genetic ablation of the *sinus venosus* EC lineage results in compensation from the endocardial EC lineage (Sharma et al., 2017b). Endocardium- and *sinus venosus*-derived EC progenitors, converge to an increasingly similar state that is dictated by the local microenvironment, despite being initially transcriptionally distinct (Phansalkar et al., 2021). In addition, recent studies showed that cardiac lymphatic ECs predominately originate from two lineages, namely Isl1+ second heart field and Pax3+ paraxial mesoderm (PM) (Lioux et al., 2020; Stone and Stainier, 2019), which further increases the spectrum of developmental origins of ECs in the heart.

Endothelial cells in the intramyocardial capillaries, or iECs, constitute a specialized barrier between the blood and the myocardium. They deliver oxygen and essential

nutrients, specifically fatty acids, to the cardiomyocytes to fulfill high energy demands of the working myocardium (Brutsaert, 2003). Endocardial ECs (eECs) form the lining of the inner surface in the ventricles and atria and play important roles during the development of working myocardium, such as formation of trabeculae network and compaction of the myocardium (Qu et al., 2022). Analysis of developing mouse heart identified markers that distinguish eECs and iECs (Iso et al., 2018; Zhang et al., 2016a). Recent single-cell RNA sequencing (scRNA-seq) studies of the human fetal heart confirmed that some of the markers identified in mouse are conserved in human, including *CD36* and *FABP5* for iECs and *NPR3* and *CDH11* for eECs, among others (McCracken et al., 2022; Miao et al., 2020).

Human pluripotent stem cells (hPSCs) represent a valuable *in vitro* model to study early stages of human development, including the heart (Hofbauer et al., 2021a). Over the past several years, protocols to differentiate cardiac cell types from hPSCs, such as different sub-types of cardiomyocytes, epicardial cells, cardiac fibroblasts and ECs were developed (Thomas et al., 2022). Engineered multicellular cardiac tissues can be generated by combining these different cell types (Campostrini et al., 2021). These have proved useful to investigate the contribution of non-cardiac cell types to cardiomyocyte cell maturation and disease (Giacomelli et al, 2020a). In addition, methods to create multicellular cardioids from hPSCs have been developed to model embryonic stages from self-organized cardiac and foregut structures to early morphogenesis during heart tube formation (Drakhlis et al., 2021; Hofbauer et al., 2021b; Lewis-Israeli et al., 2021; Silva et al., 2021). Recent studies showed that by following a specialized developmental program, hPSCs can be differentiated into ECs from several developmental lineages, such as extra- and intraembryonic hemogenic ECs (Ditadi et al., 2015; Ng et al., 2016; Uenishi et al., 2014), endocardial ECs (Mikryukov et al., 2021) and liver sinusoidal ECs (Gage et al., 2020). We previously developed a method to co-differentiate cardiomyocytes and ECs from hPSCs from cardiac mesoderm (Giacomelli et al., 2017). These hPSC-derived ECs expressed a number of cardiac specific genes like *MEOX2*, *GATA4*, *GATA6* and *ISL1*, while tissue specific endocardial or intramyocardial markers were still absent, likely because of the lack of local microenvironmental cues.

Recently, we established a three-dimensional (3D) cardiac microtissue (MT) model composed of ECs, cardiomyocytes and cardiac fibroblasts, all derived from hiPSCs (Giacomelli et al., 2020). We showed that hPSC-derived cardiomyocytes in cardiac 3D MTs showed enhanced functional and structural maturation via interaction with ECs and cardiac fibroblasts. We further showed that developmental origin of the fibroblasts was critical in this model, as cardiac-, but not skin-, fibroblasts supported cardiomyocyte maturation in 3D MTs.

However, whether 3D cardiac MTs actually induce organ-specific characteristics and to a what extent the developmental origin of ECs plays a role has not been investigated. We therefore aimed here to address these questions by comparing ECs derived from two distinct mesoderm sub-types: MESP1+ cardiac mesoderm and PAX3+ paraxial mesoderm. To do this, we utilized our earlier protocol to differentiate cardiac mesoderm-derived ECs (Giacomelli et al., 2017) and developed a new protocol to differentiate ECs from paraxial mesoderm. Cardiac MTs were then generated using these two sources of ECs. Although newly differentiated ECs from the two origins showed distinct identities, they strikingly became more similar after extended culture in cardiac MTs. Furthermore, based on eEC- and iEC-specific signatures extracted from a published scRNA-seq dataset of human fetal heart (Asp et al., 2019), we observed an iEC rather than an eEC identity for both developmental origins after MT culture. In summary, this study shows that although certain characteristics are inherited from progenitors, ECs are “plastic” and efficiently adapt to the microenvironment to acquire new tissue-specific signatures. Our results provide new insights into how organ/tissue-specific cell identities are acquired; this will inform the preparation of hiPSC -derived, organ specific ECs for disease modeling and drug development but as importantly, will provide a platform for understanding how EC plasticity might be regulated by microenvironmental context.

RESULTS

Differentiation of endothelial cells from cardiac and paraxial mesoderm

132 We set out to derive ECs from human induced pluripotent stem cells (hiPSCs) via both
133 cardiac and paraxial mesoderm intermediates. To obtain ECs from cardiac mesoderm
134 (CMECs), we used a protocol established previously in our group (Giacomelli et al.,
135 2017) (Figure 1A). Briefly, BMP4 (20 ng/ml), Activin A (ACTA, 20 ng/ml) and
136 CHIR99021 (CHIR, 1.5 μM) were used to induce cardiac mesoderm from day 0 till day
137 3. XAV-939 (XAV, 5 μM) and VEGF (50 ng/ml) were used to induce CMECs and early
138 cardiomyocytes (CMs) from day 3 to day 6. For paraxial mesoderm-ECs (PMECs), we
139 adapted a protocol developed by Loh et al. (Loh et al., 2016)(Figure 1B). Briefly, high
140 CHIR (8 μM) was used for the first two days followed by XAV (5 μM) for one day to
141 induce posterior presomitic mesoderm (pPSM) on day 3 and low CHIR (1.5 μM) was
142 used to induce anterior presomitic mesoderm (aPSM) from day 3 to day 5. VEGF was
143 added to induce PMECs from day 5 to day 6. In order to characterize paraxial
144 mesoderm differentiation and the PMEC lineage we established a double fluorescent
145 hiPSC reporter line (NCRM1 PAX3^{Venus}MSGN1^{mCherry}) (Figure S1A). CRISPR/Cas9
146 assisted gene editing was used to target the fluorescent protein Venus to the PAX3
147 locus leading to transcriptional control by the endogenous PAX3 regulatory elements.
148 The MSGN1^{mCherry} reporter was generated using a BAC construct integrated into the
149 cells using the piggyBac transposon system. Flow cytometry analysis at different
150 stages of paraxial mesoderm differentiation showed efficient induction of pPSM
151 (MSGN-mCherry positive cells) and aPSM (PAX3-Venus positive cells) on day 2-3
152 and day 5, respectively (Figure S1B). Using our paraxial mesoderm protocol, more
153 than 70% of cells acquired MSGN1-mCherry expression on day 2-3 (Figure S1C) and
154 more than 50% of cells acquired PAX3-Venus on day 6 (Figure S1D). We next
155 confirmed induction of endogenous PAX3 protein expression by immunostaining with
156 a PAX3-specific antibody (Figure S1E). Notably, more than 90% of cells were positive
157 for PAX3 on day 5; this could be because of relatively weak endogenous expression
158 of Venus that could not be detected in PAX3^{low} cells.
159
160 Gene expression analysis further confirmed comparable expression of pan-mesoderm
161 markers *TBXT* and *MIXL1* in both cardiac and paraxial mesoderm differentiation
162 conditions. On the other hand, expression of cardiac genes (*MESP1*, *GATA4* and
163 *NKX2-5*) was restricted to cardiac mesoderm differentiation conditions and expression

164 of paraxial mesoderm genes (*MSGN1*, *TBX6*, *PAX3*) was restricted to paraxial
165 mesoderm differentiation conditions (Figure S1F).
166
167 Both cardiac and paraxial mesoderm differentiation conditions resulted in comparable
168 percentages of CD144+CD140a- ECs on day 6 and day 8 of differentiation (Figure
169 1C-D). CD144+CD140a- ECs were sorted on day 6 and day 8 of differentiation from
170 both cardiac and paraxial mesoderm conditions and underwent RNA sequencing
171 (RNA-seq). Principle component analysis (PCA) showed that CMECs and PMECs
172 clustered separately along PC1, and day 6 and day 8 were separated along PC2
173 (Figure 1E). On day 6, 3307 and 2592 genes were significantly differentially
174 upregulated (FDR<0.05, fold-change>2) in CMECs and PMECs respectively (Table
175 S1). Gene ontology (GO) analysis showed that cardiac related genes were specifically
176 upregulated in day 6 CMECs (CMEC_D6), while genes related to skeletal system
177 development and function were specifically upregulated in day 6 PMECs (PMEC_D6)
178 (Figure 1F, Table S2). Genes involved in heart development, like *GATA4*, *GATA5*,
179 *TBX3*, *ISL1* and *MYH6*, were highly expressed in day 6 and day 8 CMECs. *TBX3*,
180 *ISL1* and *MYH6* were upregulated from day 6 to day 8 in CMECs (Figure 1G).
181 Essential genes for skeletal muscle development like *PAX3*, *TBX1*, *FOXC1*, *EYA1* and
182 *MEOX1* were largely expressed in day 6 and day 8 PMECs. *FOXC1* and *EYA1* were
183 upregulated from day 6 to day 8, while *TBX1* and *MEOX1* were downregulated (Figure
184 1G). In summary, unbiased expression analysis by bulk RNA-seq showed differential
185 gene expression signatures of cardiac and paraxial mesoderm derived ECs that
186 corresponded to their known expression profiles *in vivo*.
187
188 **Reconstruction of the differentiation trajectories of ECs by single-cell RNA-seq**
189
190 Having demonstrated that the two differentiation protocols result in ECs with distinct
191 characteristics, we undertook an unbiased analysis of the complete cell population
192 and reconstructed the EC differentiation trajectories. To this end, we performed
193 scRNA-seq on day 6 of CMEC and PMEC differentiation from two independent
194 biological replicates (Figure 2A-B, Figure S2A-B). The replicates appeared highly
195 similar in a low-dimensional representation (Figure S2C) and were therefore combined
196 for further analysis. Any remaining, undifferentiated hiPSCs were excluded from

197 further analysis (Figure S2D-E). In the CMEC differentiation data set, cells were
198 grouped into 3 clusters (cardiac mesoderm, cardiomyocytes and CMECs), as
199 established previously (Cao et al., 2022) (Figure 2C). The three cell types were
200 identified by known marker genes (Figure 2D, S3A-B, Table S3). The cardiac
201 mesoderm cluster was characterized by mesoderm and early cardiac genes, such as
202 *MESP1, SMARCD3, ABLIM1, TMEM88, ISL1, MYL5,* as well as the cell cycle-related
203 genes *CDK6* and *NEK2*. The CMEC cluster was characterized by EC markers (*CDH5,*
204 *CD34, KDR, HEY2, TEK, TIE1, ACVRL1, SOX17, ENG, ICAM2, PECAM1)*.
205 Cardiomyocytes were identified by expression of cardiomyocyte-associated genes,
206 including *MYL4, TNNI1, MYL7, ACTA2, TNNT2, HAND2* and *NKX2-5*. To reveal the
207 differentiation trajectories of the cells, we calculated the diffusion pseudotime using a
208 cardiac cell mesoderm cell as root (Figure 2E). Pseudotime increased towards
209 CMECs and cardiomyocytes, suggesting that both cell types differentiated from a
210 common cardiac mesoderm progenitor.
211
212 In the PMEC differentiation data set, all cells were divided into 3 clusters (Figure 2F),
213 which were interpreted as being paraxial mesoderm, PMECs and mixed lateral plate
214 mesoderm (LPM)/sclerotome using marker gene analysis (Figure S3C, D, Table S4).
215 The paraxial mesoderm cluster was characterized by expression of aPSM and
216 dermomyotome genes, such as *MEOX1, PDGFRB, SIX1, CRABP2, NR2F1, EYA1,*
217 *FOXC1 and PAX3*. PMECs were characterized by EC markers, like *ETV2, CDH5,*
218 *CD34, KDR, ENG, SOX17, PLVAP, APLN, NRP1*. The mixed LPM/sclerotome cluster
219 was characterized by LPM and sclerotome specific genes, such as *TMEM88*, *HAND1,*
220 *TNNI1, PRRX1, ACTA2, DES, FOXH1, LEF1* and *JAG1* (Figure 2G, S3C-D). Diffusion
221 pseudotime rooted in the paraxial mesoderm increased towards both PMECs and
222 LPM/Sclerotome (Figure 2H). Both cell types therefore likely differentiated from a
223 common paraxial mesoderm progenitor.
224
225 **Acquisition of an organ-specific identity in cardiac microtissues**
226
227 Being able to produce ECs with properties corresponding to their mesodermal origins
228 enabled us to test in how far the cellular microenvironment can either reinforce or
229 reverse this specification i.e. how “plastic” the ECs are. Specifically, we set out to

230 mimic the cardiac microenvironment *in vitro* using a protocol for creating cardiac MTs,
231 published previously by our group (Giacomelli et al., 2020). Briefly, CD34+ CMECs or
232 PMECs were sorted on day 6 and combined with hiPSC-derived cardiomyocytes
233 (hiPSC-CMs) and hiPSC-derived fibroblasts (hiPSC-CFs) in a ratio of 15:70:15 to form
234 MTs. MTs made from CMECs (CM_MTs) and PMECs (PM_MTs) were collected after
235 21 days from two independent biological replicates by scRNA-seq (Figure 3A, Figure
236 S2A-B). The replicates appeared highly similar in a low-dimensional representation
237 (Figure S2C) and were therefore combined for further analysis. Any remaining,
238 undifferentiated hiPSCs were excluded from further analysis (Figure S2F-G). Both
239 CM_MTs and PM_MTs datasets were divided into three clusters that correspond to
240 hiPSC-CFs, hiPSC-CMs and hiPSC-ECs (Figure 3B). Marker genes identified for each
241 cluster, confirmed the cluster identities (Table S6).
242
243 In order to assess to what extent ECs in MTs acquired an organ-specific identity, we
244 compared their expression profiles to primary ECs in a published data set of the
245 human fetal heart (Asp et al., 2019) (Figure S4A). In this data set, we reannotated the
246 original endothelium/pericytes/adventia cluster (cluster 10) as intramyocardial ECs,
247 based on differentially expressed markers such as *A2M, CD36, APLNR, ARHGAP18,*
248 *IGFBP3, CLDN5, FABP4* and *FABP5* (Figure S4B, Table S5). The cluster annotated
249 as capillary endothelium (cluster 0) in the original publication was reannotated as
250 endocardium, due to the presence of differentially expressed markers like *NPR3,*
251 *ALDH2, CDH11, ECE1, TMEM100, FOXC1* and *EDN1* (Figure S4B, Table S5).
252 Supporting the differential expression test, UMAP visualization of representative intra-
253 myocardial and endocardial markers showed specific expression in the respective
254 clusters (Figure S4C-D).
255
256 We next compared CMECs and PMECs on day 6 of differentiation (CMECs_day 6 and
257 PMECs_day 6) with the CMECs and PMECs in MTs (CMECs_MT and PMECs_MTs)
258 respectively. CMECs in MTs upregulated expression of intramyocardial makers, such
259 as *CLDN5, GMFG, APLNR, CD36, NOTCH4, OIT3, IGFBP3, ARHGAP18, A2M* and
260 *BCAM*, but not *FABP5*, compared to CMECs isolated on day 6 of differentiation (Figure
261 3C,D, Table S7). PMECs in MTs upregulated expression of a few intramyocardial
262 markers, such as *CLDN5, GMFG, NOTCH4, IGFBP3, ARHGAP18, A2M* and *BCAM*,

263 but not *APLNR, CD36, OIT3* and *FABP5* compared to PMECs isolated on day 6 of
264 differentiation (Figure 3C,E, Table S7). We also found some endocardial markers
265 upregulated in both CMECs and PMECs in MTs (*TFPI2, EDN1, ECE1, FOXP1*)(S5A-
266 B, Table S7). However, the differences in endocardial marker expression were smaller
267 compared to intramyocardial markers. Notably, the expression of several
268 intramyocardial markers, especially *APLNR, CD36, OIT3, ARHGAP18, A2M, BCAM*
269 and *FABP5* was higher in CMECs in MTs compared to PMECs in MTs (Figure 3F,
270 Table S8). Although the expression of endocardial markers was also higher in CMECs
271 in MTs compared to PMECs in MTs, their average expression levels were lower in
272 general when compared to intramyocardial markers (Figure S5C, Table S8).
273 Importantly, endocardial makers, including *CDH11, FOXC1, FZD6, TMEM100* and
274 *NPR3,* were barely expressed in either CMECs or PMECs in MTs (Figure S5C).
275 Overall, intramyocardial EC identify was acquired by all hiPSC-ECs in the cardiac MT
276 environment.
277
278 **Distinct cell identities are preserved in cardiac microtissues composed of either**
279 **cardiac or paraxial mesoderm-derived ECs**
280
281 To obtain a clearer view of the similarities between ECs in MTs and primary fetal heart
282 ECs, we merged the CM_MT and PM_MT datasets with the human fetal heart dataset
283 (Asp et al., 2019) (Figure 4A-B). In the case of both the CM_MT and the PM_MT
284 dataset, we found that CFs in MTs (CF_MT) clustered together with fetal heart
285 fibroblast-like cells and CMs in MTs (CM_MT) clustered together with fetal heart
286 ventricular CMs. Notably, both CMECs in MTs (CMECs_MT) and PMECs in MTs
287 (PMECs_MT) clustered together with fetal heart intramyocardial ECs and not
288 endocardium (Figure 4A-D). To quantify our observation, we calculated the distances
289 (in expression space) between each cell in MTs and the fetal heart dataset. This
290 calculation showed that CF_MT cells are closest to fibroblast-like cells *in vivo* (related
291 to cardiac skeleton connective tissue), CM_MT cells are closest to ventricular
292 cardiomyocytes and CMECs_MT as well as PMECs_MT are closest to intramyocardial
293 ECs in human fetal heart (Figure 4E). Annotating the *in vitro* cells based on the closest
294 *in vivo* neighbors revealed that cell type identities were very similar in CM_MTs and
295 PM_MTs (Figure 4E).

296

297 Correspondingly, the set of markers of the EC cluster in CM_MTs and the PM_MTs,
298 CM_MTs (ECs) and PM_MT (ECs) respectively, showed a high overlap (Jaccard
299 similarity) with the markers of intra-myocardial ECs we extracted from the *in vivo* data
300 set (Figure 4F). The gene set upregulated in CMECs_MT compared to CMECs_day 6
301 (Up in CMECs_MTs) had a higher overlap with intramyocardial EC markers than the
302 set of genes upregulated in PMECs_MTs compared to PMECs_day 6 (Up in
303 PMECs_MTs) (Figure 4F). For comparison, we also profiled CMECs that were
304 cultured for two additional passages in monoculture. Genes that were upregulated in
305 these cells compared to CMECs_day 6 (Up in P2 CMECs) overlapped the least with
306 intra-myocardial EC markers (Figure 4F). This result excludes the possibility that the
307 effects observed in MTs are simply due to environment-independent differentiation
308 progression over time. CMECs_MT and PMECs_MT thus both resembled
309 intramyocardial ECs but a difference between the two differentiation methods
310 remained. To quantify this difference directly, we used differential gene expression
311 analysis. On day 6 of differentiation, 1446 genes were differentially expressed
312 between CMECs and PMECs (Table S9), while only 332 genes were differentially
313 expressed between CMECs_MT and PMECs_MT (Table S8). 81 genes were shared
314 between the two sets and 251 genes were differentially expressed only between
315 CMECs_MT and PMECs_MT (Figure 4G). Intramyocardial marker genes (*CD36*, *OIT3*,
316 *A2M*, *CLDN5*, *APLNR*, *FABP5*) were among these 251 genes that were differentially
317 expressed between the CMECs_MT and PMECs_MT. This is also in line with our
318 observations that expression of some intramyocardial marker genes were higher in
319 CMECs in MTs compared to PMECs in MTs. Next, all EC clusters from bulk and single
320 cell RNA-seq datasets were combined and visualized using principal component
321 analysis (PCA) (Figure 4H). CMECs_day 6 and PMECs_day 6 clustered far apart,
322 while CMECs_MT and PMECs_MT clustered closely together. Bulk and single cell
323 RNA-seq samples clustered together for both CMECs and PMECs. CMECs_MT and
324 PMECs_MT were found closer to fetal heart intramyocardial ECs and fetal heart ECs
325 (Figure 4H) sequenced in our previous study (Giacomelli et al., 2020). Altogether,
326 analysis of the *in vitro* and *in vivo* data sets demonstrated that the cardiac tissue
327 microenvironment resulted in hiPSC-ECs acquiring an intramyocardial EC identity

independent of their developmental origin and, further, gene expression differences due to distinct mesodermal origins were partially removed.

DISCUSSION

In the present study we derived ECs from hiPSCs from two mesoderm lineages namely LPM and PM, as previous lineage tracing studies have shown that LPM and PM serve as a major source of ECs in the developing embryo (Lagha et al., 2009; Mayeuf-Louchart et al., 2016; Pardanaud et al., 1996). We showed that ECs isolated on day 6 and day 8 of differentiation retained their developmental lineage history. Transcription factors involved in the heart and skeletal muscle development were highly expressed in CMECs and PMECs, respectively. Additional approaches, including scRNA-seq, showed lineage diversification from a common cardiac and paraxial mesoderm progenitor during differentiation of CMECs and PMECs, respectively. At the same time, an organ-specific EC signature was absent in ECs differentiated either from cardiac or paraxial mesoderm on day 6 and day 8 of differentiation, or upon extended culture.

Local microenvironmental cues result in acquisition of organ-specific characteristics in ECs (Aird, 2012). To model the influence of cell-extrinsic factors, we took advantage of our cardiac MT model which mimics the heart-specific microenvironment, as it integrates CMs, CFs and ECs (Giacomelli et al., 2020). Although both CMECs and PMECs acquired an iEC identity after incorporation into MTs, several intramyocardial EC markers *(APLNR, CD36, OIT3, ARHGAP18, A2M, BCAM* and *FABP5*) were more strongly upregulated in CMECs compared to PMECs in cardiac MTs. A recent study in mouse embryos showed that transcriptional heterogeneity in the sinus venosus (SV) and endocardium-derived iECs declines over time (Phansalkar et al., 2021). Therefore, it would be interesting to investigate whether PMECs require longer culture in cardiac MTs to acquire comparable expression of intramyocardial EC markers as in CMECs. On the other hand, endocardial markers were not detected in either CMECs or PMECs in cardiac MTs. This is in line with previous evidence that the cardiac MTs microenvironment recapitulates myocardial and not endocardial layers of the heart. Importantly, CFs and CMs in both CM_MT and PM_MT datasets were highly similar and clustered together with fetal heart fibroblast-like cells and fetal heart ventricular

361 CMs respectively. This showed that developmental origin of ECs does not influence
362 CF or CM identities in cardiac MTs.
363
364 Among EC lineages, PM serves a source of lymphatic ECs in the heart, skin and lymph
365 node (Lenti et al., 2022; Lupu et al., 2022; Stone and Stainier, 2019). PMECs showed
366 increased expression of genes important for the development of lymphatic vasculature,
367 such as *TBX1, FOXC1, LYVE1, VEGFC.* At the same time, expression of the master
368 regulator of lymphatic EC differentiation (*PROX1*) was not detected in PMECs either
369 at day 6 or in cardiac MTs. It would be interesting to explore whether addition of known
370 lymphatic EC growth factors promotes *PROX1* expression in PMECs.
371
372 Genetic lineage tracing in mice has identified a variety of developmental origins for
373 organ-specific ECs in different tissues. However, whether developmental origin is a
374 prerequisite- or simply a default developmental route remains an open question. On
375 the other hand, the present and previous studies demonstrate that local
376 microenvironmental cues might play a bigger role in not only the acquisition but also
377 the maintenance of the organ-specific characteristics. This is also in line with recent
378 study on sinusoidal ECs of the liver (Gómez-Salinero et al., 2022). Earlier studies have
379 demonstrated the importance of the *Gata4* transcription factor in the differentiation of
380 liver ECs and the acquisition of sinusoidal-like identity (Géraud et al., 2017; Zhang et
381 al., 2016b). However, scRNA-seq analysis of liver ECs showed that *Gata4* is not
382 restricted to sinusoidal ECs but it is expressed by all ECs in the liver (Gómez-Salinero
383 et al., 2022). Instead, the *c-Maf* transcription factor was restricted to sinusoidal liver
384 ECs and was regulated by BMP9 that is highly expressed by hepatic stellate cells
385 (HSC) (Breitkopf-Heinlein et al., 2017). Furthermore, overexpression of c-Maf was
386 sufficient to induce sinusoidal-like characteristics in human umbilical vein ECs
387 (HUVECs). The same is true for heart ECs that are derived from multiple
388 developmental pools of EC progenitors that converge to a similar state over time
389 (Milgrom-Hoffman et al., 2011; Phansalkar et al., 2021; Sharma et al., 2017b).
390
391 In summary, we demonstrated that ECs, derived from two distinct mesoderm lineages
392 namely LPM and PM, acquire organ-specific characteristics upon incorporation into
393 the cardiac MT environment which includes CMs and CFs. We expect that our findings

394 will guide the derivation of organ-specific ECs from hiPSCs in the future and lay the
395 foundation for various biomedical applications, from creating of disease models to
396 transplantation therapies.
397
398 **Materials and Methods**
399 **hiPSC culture**
400 hiPSC lines LUMC0020iCTRL-06 and NCRM1 (NIH Center for Regenerative Medicine
401 NIH CRM, obtained from RUDCR Infinite Biologics at Rutgers University) were
402 cultured in in TeSR-E8 on Vitronectin XF and were routinely passaged once a week
403 using Gentle Cell Dissociation Reagent (all from Stem Cell Technologies, Vancouver,
404 Canada).
405
406 **Generation of PAX3^{Venus}MSGN1^{mCherry} hiPSC dual reporter line**
407 Prior to targeting, NCRM1 hiPSCs were passaged as a bulk on feeders in hESC-
408 medium (Costa et al., 2007). RevitaCell (Life Technologies, Carlsbad, CA, USA) was
409 added to the medium (1:200) after every passage to enhance viability after single cell
410 passaging with TrypLE (Life technologies). PAX3^{Venus} was generated by
411 CRISPR/Cas9 as follow: NCRM1 hiPSCs were passaged with ratio 1:3 into 60 mm
412 dishes to reach 60-70% confluency the next day for transfection. Cells were
413 transfected with pCas9-GFP (Addgene plasmid #44719), pBR322-U6-hPAX3-gRNA-
414 S1 containing sgRNA CCGGCCAGCGTGGTCATCCT and repair template p15A-cm-
415 hPAX3-Venus-neo-1kb containing a Venus-neo cassette with 1 kb hPAX3 homology
416 arms. The antibiotic selection marker is flanked by FRT sites for Flp-mediated
417 excision. 20 µl lipofectamine (Invitrogen, Waltham, Massachusetts, USA), 8 µg of
418 pCas9-GFP, 8 µg of sgRNA plasmid and 8 µg of linearized repair template were
419 diluted in 600 µl of Opti-MEM and added to each 60 mm dish. After 18 hours the
420 medium was changed to hESC medium. After another 6 hours G-418 (50 µg/ml)
421 selection was started and was kept for 1 week. Surviving cells were cultured in hESC
422 medium, passaged and transferred into 6-well plates for the transfection of Flp
423 recombinase expression vector to remove the neomycin cassette. 300 µl of Opti-MEM
424 containing 10 µl lipofectamine and 4 µg CAGGs-Flpo-IRES-puro plasmid was added
425 per well for 18 hours. Puromycin (0,5 µg/ml) selection was started 24 hours post
426 transfection and lasted for 2 days. Once recovered, cells were passage into 96-well

427 format for clonal expansion via limited dilution. Targeted clones were identified by PCR
428 and Sanger sequencing (BaseClear, Leiden, Netherlands). The MSGN1^{mCherry} reporter
429 line was generated by Transposon mediated BAC transgenesis using protocols
430 described by (Rostovskaya et al., 2012). In brief, a human BAC (RP11-12L16) with
431 piggyBac transposon repeats flanking the bacterial backbone and with mCherry
432 inserted directly after the initiating Methionine of MSGN1 was transfected together with
433 a piggyBac Transposase into NCRM1 hiPSCs.
434
435 **Differentiation of ECs from cardiac and paraxial mesoderm**
436 ECs from cardiac mesoderm were differentiated as previously described (Giacomelli
437 et al., 2017). ECs from paraxial mesoderm were differentiated using a modified Loh et
438 al. protocol (Loh et al., 2016). Briefly, 5 x 10^4 cells per cm^2 were seeded on plates
439 coated with 75 µg/mL Matrigel (growth factor reduced) (Corning) the day before
440 differentiation (day -1). At day 0, paraxial mesoderm was induced by changing TeSR-
441 E8 to BPEL (Bovine Serum Albumin [BSA], Polyvinyl alcohol, Essential Lipids)
442 medium (Ng et al., 2008), supplemented with 8 µM CHIR99021. At day 2, cells were
443 refreshed with BPEL supplemented with 5 µM XAV939. At day 3, cells were refreshed
444 with BPEL supplemented with 4 µM CHIR99021. From day 5 onwards, cells were
445 refreshed every 3 days with BPEL medium supplemented with 50 ng/ml VEGF.
446
447 **Fluorescence-activated cell sorting**
448 Cells were dissociated with TrypLE on day 6 and 8 of CMEC and PMEC protocol and
449 stained with VE-Cadherin PE-conjugated Antibody (R&D Systems). Then VEC+ cells
450 were sorted using FACSAria III. Total RNA was extracted right after sorting using the
451 NucleoSpin® RNA kit (Macherey-Nagel, Düren, Germany).
452
453 **Generation of 3D Cardiac Microtissues (MTs)**
454 Cardiac MTs were generated from hiPSC-derived ECs, CFs and CMs as previously
455 described (Giacomelli et al., 2020). Briefly, on day 6 of CMEC and PMEC
456 differentiation, $CD34^+$ ECs were isolated using a Human cord blood CD34 Positive
457 selection kit II (StemCell Technologies) following the manufacturer's instructions. On
458 the day of MT formation, freshly isolated hiPSC-ECs and cultured hiPSCs-CFs and
459 hiPSC-CMs were combined together to 5000 cells (70% cardiomyocytes, 15%

460 endothelial cells and 15% cardiac fibroblasts) per 50µl BPEL medium supplemented
461 with VEGF (50 ng/ml) and FGF2 (5 ng/ml). Cell suspensions were seeded on V-bottom
462 96 well microplates (Greiner bio-one, Kremsmünster, Austria) and centrifuged for 10
463 min at 1100 rpm. MTs were incubated at 37ºC, 5% CO_2 for 21 days with media
464 refreshed every 3-4 days. scRNAseq analysis of MTs was performed after 21 days.
465

466 **Fluorescence-activated cell sorting**

467 Cells were detached using TrypLE for 5 min at 37°C and washed once with FACS
468 buffer (PBS containing 0.5% BSA and 2 mM EDTA). Primary antibodies CD144 (1:50,
469 eBioscience), CD140a (1:20, BD Bioscience) were added for 1 hr at 4ºC. Samples
470 were measured on MACSQuant VYB (Miltenyi Biotech) equipped with a violet (405
471 nm), blue (488 nm) and yellow (561 nm) laser. The results were analyzed using Flowjo
472 v10 (FlowJo, LLC). For FACS sorting on day 6 and day 8 of the CMEC and PMEC
473 protocol, CD144+CD140a- cells were sorted using FACSAria III (BD-Biosciences).
474

475 **Quantitative Real-Time Polymerase Chain Reaction (qPCR)**

476 Total RNA was extracted using the NucleoSpin® RNA kit according to the
477 manufacturer's protocol. cDNA was synthesized using an iScript-cDNA Synthesis kit
478 (Bio-Rad, Hercules, CA, USA). iTaq Universal SYBR Green Supermixes (Bio-Rad)
479 and Bio-Rad CFX384 real-time system were used for the PCR reaction and detection.
480 Relative gene expression was determined according to the standard ΔCT calculation
481 and normalized to the housekeeping gene RPL37A.
482

483 **Bulk RNA sequencing and analysis**

484 Bulk RNAseq of passage two CMECs (CMECs P2) and human fetal heart ECs at
485 gestation age Week(W)12.5, W15 and W21 were performed in our previous study
486 (Giacomelli et al., 2020) and obtained from GEO accession number GSE116464.
487 Bulk RNAseq of day 6 and 8 of CMEC and PMEC differentiation were performed at
488 BGI (Shenzhen, China) using the Illumina Hiseq4000 (100bp paired end reads). Raw
489 data was processed using the LUMC BIOPET Gentrap pipeline
490 (https://github.com/biopet/biopet), which comprises FASTQ preprocessing, alignment
491 and read quantification. Sickle (v1.2) was used to trim low-quality read ends
492 (https://github.com/najoshi/sickle). Cutadapt (v1.1) was used for adapter clipping

493 (Martin, 2011), reads were aligned to the human reference genome GRCh38 using
494 GSNAP (gmap-2014-12-23) (Wu and Nacu, 2010; Wu and Watanabe, 2005) and gene
495 read quantification with htseq-count (v0.6.1p1) against the Ensembl v87 annotation
496 (Yates et al., 2015). Gene length and GC content bias were normalized using the R
497 package cqn (v1.28.1) (Hansen et al., 2012).Genes were excluded if the number of
498 reads was below 5 reads in ≥90% of the samples.
499
500 Differentially expressed genes were identified using generalized linear models as
501 implemented in edgeR (3.24.3) (Robinson et al., 2009). P-values were adjusted using
502 the Benjamini-Hochberg procedure and FDR ≤ 0.05 was considered significant.
503 Analyses were performed using R (version 3.5.2). PCA plot was generated with the
504 built-in R functions prcomp using transposed normalized RPKM matrix. Correlation
505 among samples was calculated using cor function with spearman method and the
506 correlation heatmap was generated with aheatmap function (NMF package). Gene
507 ontology enrichment was performed using compareCluster function of clusterProfiler
508 package (v3.10.1) (Yu et al., 2012) and q ≤ 0.05 was considered significant.
509
510 **Single-cell RNA sequencing and analysis**
511 **Library preparation and sequencing**
512 Library preparation was performed as previously described (Giacomelli et al., 2020).
513 Briefly, single cells were loaded into the 10X Chromium Controller for library
514 construction using the Single-Cell 3' Library Kit, Version 2 Chemistry (10x Genomics,
515 Pleasanton, CA, USA) according to the manufacturer's protocol. Next, indexed cDNA
516 libraries were sequenced on the HiSeq4000 platform. Single-cell expression was
517 quantified using unique molecular identifiers (UMIs) by 10x Genomics' "Cell Ranger"
518 software.
519
520 The mean reads per cell for all eight data sets: CMEC (R1): 28,499; CMEC (R2):
521 29,388; PMEC (R1): 31,860; PMEC (R2): 38,415; CM_MT (R1): 39,319; CM_MT (R2):
522 29,741; PM_MT (R1): 36,726; PM_MT (R2): 26,421.
523
524 **Single-cell RNAseq data pruning and normalization**

525 For data pruning and normalization, the two replicates of each of the 4 conditions
526 (CMEC, PMEC, CM_MT and PM_MT) were combined without batch correction. Then,
527 cells with a low number of genes per cell (1200 [CMEC], 1200 [PMEC], 900 [CM_MT],
528 750 [PM_MT], see Fig. S2A-B) were removed. Genes expressed in less than 2 of the
529 remaining cells with a count of at most 1 were excluded from further analysis. Each
530 combined data set was normalized using the R package scran (V 1.14.6) (Lun et al.,
531 2016). Highly variable genes (HVGs) were calculated (improvedCV2 from the scran
532 package) for each replicate of the combined data sets after excluding ribosomal genes
533 [Ribosomal Protein Gene Database], stress markers (Brink et al., 2017) and
534 mitochondrial genes. For downstream analysis the top 5% HVGs were used after
535 excluding proliferation (Whitfield et al., 2006) and cell cycle (Giotti et al., 2017) related
536 genes.
537
538 **Cell cycle analysis and batch correction**
539 For each combined data set, cell cycle analysis was performed with the scran package
540 using the cyclone function (Scialdone et al., 2015) on normalized counts (Figure S2H).
541 Cells with a G2/M score higher than 0.2 were considered to be in G2/M phase.
542 Otherwise, they were classified as G1/S. Using this binary classifier as predictor, we
543 regressed out cell cycle effects with the R package limma (V 3.42.2) (Ritchie et al.,
544 2015) applied to log-transformed normalized counts. Then, for each combined data
545 set, the two replicates were batch corrected with fast mutual nearest neighbors
546 correction method (MNN) (Haghverdi et al., 2016) on the cell cycle corrected counts,
547 using the 30 first principal components and 20 nearest-neighbors (Figure S2C).
548
549 **Clustering**
550 For each combined data set, batch-corrected counts were standardized per gene and
551 then used to create a shared nearest neighbour (SNN) graph with the *scran* R package
552 (d = 30, k = 2). Louvain clustering was applied to the SNN graph using the *igraph*
553 python package (V 0.7.1) with these resolution parameters: 0.4 [CMEC], 0.4 [CM_MT],
554 0.3 [PMEC], 0.1 [PM_MT]. For the CMEC data set, this resulted in 5 clusters (Figure
555 S2D). Two of these 5 clusters were excluded from further analysis based on the
556 expression of pluripotency markers (Figure S2E). For the PMEC data set, this resulted
557 in 3 clusters (Figure 2F). For CM_MT and PM_MT, clustering resulted in 4 clusters

558 (Figure S2F and S2G), where one cluster was excluded from further analysis, because
559 it was mainly present in one of the two replicates. Additionally, the attempt to map this
560 cluster to in vivo data, resulted in mostly unassigned cell types (plot not shown). For
561 PMEC, clustering resulted in 3 clusters.
562
563 **Dimensionality reduction and pseudotime**
564 Dimensionality reduction was performed using the python *scanpy* pipeline (V 1.4.6).
565 For both data sets, CMEC and PMEC, a 20 nearest-neighbors (knn, k=20) graph was
566 created from diffusion components of the batch corrected data sets. Diffusion
567 components are the eigenvectors of the diffusion operator which is calculated from
568 Euclidean distances and a gaussian kernel. The aim is to find a lower dimensional
569 embedding which considers the cellular progression. Both graphs were projected into
570 two dimensions with the default force-directed graph layout and starting positions
571 obtained from the partition-based graph abstraction (PAGA) output (Wolf et al., 2019).
572 PAGA estimates connectivities between partitions and performs an improved version
573 of diffusion pseudotime. Diffusion pseudotime (Haghverdi et al., 2016; Wolf et al.,
574 2019) was calculated on these graphs with root cells selected based on the graph
575 layout from the "Cardiac Mesoderm" cluster in CMEC, and the "Paraxial Mesoderm"
576 cluster in PMEC.
577
578 For CM_MT and PM_MT, the knn graphs (k=50 for PM_MT, k=100 for CM_MT) were
579 created from the first 30 principal components of the batch corrected data sets. These
580 graphs were projected into two dimensions with the default force-directed graph layout
581 and starting positions from the PAGA output.
582
583 ***In vivo* data analysis and mapping**
584 The *in vivo* data set, downloaded from https://www.spatialresearch.org/resources-
585 published-datasets/doi-10-1016-j-cell-2019-11-025/, contains a 6.5 PCW human
586 embryonic cardiac tissue sample. The clusters and cluster annotations were obtained
587 from the original publication (Asp et al., 2019). The data set was normalized with the
588 scran R package and HVGs were calculated as described in section "Single-cell RNA-
589 seq data pruning and normalization". Dimensionality reduction was performed with the

590 R package *umap* (V 0.2.5.0) using 20 nearest-neighbors, min_dist = 0.7 and Euclidean
591 distance.
592
593 **Differential expression analysis**
594 All differential expression tests were performed with edgeR (V 3.28.1) (Robinson et
595 al., 2009) using a negative binomial regression and raw counts. The predictors in the
596 regression were: cluster and replicate (both discrete variables), as well as the total
597 number of counts per cell.
598
599 For marker gene analysis (Figures S3A and S3C), p-values were obtained for a
600 contrast between the cluster of interest and all other clusters using regression
601 coefficients averaged over the replicates. For tests between different data sets (Figure
602 3C), the corresponding endothelial cell cluster was extracted from each data set. Then,
603 a contrast between MT and day 6 was calculated by averaging over the predictors of
604 both replicates. For the *in vivo* test (Figure S4B), intra-myocardial EC and
605 endocardium clusters were extracted from the data set to calculate the contrast
606 between them. P-values were adjusted for multiple hypothesis testing with the
607 Benjamini-Hochberg method.
608
609 **Comparison to the *in vivo* data set**
610 CM_MT and PM_MT data sets were mapped on the *in vivo* data set using the MNN
611 method (d = 30 principal components, k = 100 nearest neighbors). First, *in vitro*
612 replicates were mapped to each other, then the *in vivo* data was mapped on the
613 combined *in vitro* data, using normalized, log- transformed counts and the 10% top
614 HVGs of the *in vivo* data set. Dimensionality reduction was performed with the R
615 package *umap* using 100 nearest-neighbors, min_dist = 0.3 and Euclidean distance.
616 K-nearest-neighbour (KNN) assignment was performed in the batch corrected,
617 principal component space (30 PCs). The 100 nearest-neighbors in the *in vivo* data
618 set based on Euclidean distances were calculated for each *in vitro* cell. The *in vitro*
619 cell was ascribed the cell type most abundant among the 100 *in vivo* neighbors. Each
620 such assignment received a confidence score, which is the number of *in vivo*
621 neighbors with that cell type divided by the number of all nearest neighbors (=100). A
622 cell was not ascribed a cell type if either the average distance to its nearest neighbour

exceeded a certain threshold (determined by the long tail of the histogram of average distances: 0.35), or the assignment had a confidence score less than 0.5. In addition, clusters containing less than 10 cells were not ascribed a cell type.

For the Jaccard similarity measure, marker genes of each differential expression test were selected with adjusted p-value < 0.05. The remaining genes were ranked by log2 fold change and the first 478 genes were selected for analysis. Then, the Jaccard distances were calculated between the marker genes of intra-myocardial endothelial cells and each of the other gene sets.

For principal component analysis (Figure 4H), human fetal bulk samples and in vitro bulk samples (Giacomelli et al., 2020) were combined with the single cell data sets. For each single-cell data set, the endothelial cells were extracted and the sum per gene over all cells was calculated. Then, bulk and single cell samples were log-transformed and combined into one data set. Principal component analysis was applied on the gene-wise standardized data set, using marker genes of the intra-myocardial endothelial cells from the *in vivo* data set.

Data Availability Statement

The accession numbers for the bulk and single cell RNA sequencing datasets reported in this paper are https://www.ncbi.nlm.nih. gov/geo/ GEO: GSE151427 (day 6 and day 8 CMEC and PMEC (bulk); day 6 PMEC (single cell); PM_MT (single cell)); GSE202901 (day 6 CMEC (single cell)); GSE147694 (CM_MT (single cell)).

Statistics

Statistical analysis was conducted with GraphPad Prism 7 software (San Diego, CA, USA). Data are represented as mean± SD.

Acknowledgements

This project received funding from the European Union's Horizon 2020 Framework Programme (668724); Netherlands Organ-on-Chip Initiative, an NWO Gravitation project funded by the Ministry of Education, Culture and Science of the government of

655 the Netherlands (024.003.001); the European Union's Horizon 2020 and innovation
656 program under a Marie Sklodowska-Curie grant agreement no. 707404. We thank
657 Elisa Giacomelli and Milena Bellin for generation of cardiac microtissues; S.L. Kloet
658 and E.de Meijer (Leiden Genome Technology Center) for help with 10X Genomics
659 experiments (cell encapsulation, library preparation, single-cell sequencing, pri-mary
660 data mapping, and quality control); the LUMC Flow Cytometry Core Facility, and the
661 LUMC Light and Electron Microscopy Facility. Illustrations were created with
662 BioRender.
663

664 **Author contributions**

665 X.C., M.M., S.S., V.V.O. designed the research, analyzed and interpreted results,
666 wrote the manuscript; X.C., F.E.vdH, V.V.O. performed experiments; M.M., S.S.
667 performed scRNA-Seq analysis; K.N. generated MSGN1^{mCherry} hiPSC reporter line;
668 K.A. generated gene targeting constructs for reporter hiPSC lines; X.C., H.M.
669 performed bulk RNA-seq analysis; C.L.M. designed the research and edited the
670 manuscript.
671

672 **Competing interests**

673 C.L.M. is co-founder of Ncardia bv. The other authors indicated no potential conflicts
674 of interest.
675
676
677

678 **Figure Legends**

679

680 **Figure 1. Characterization of ECs differentiated from hiPSCs using CMEC and**
681 **PMEC protocols**

682 (**A-B**) Schematic overview of CMEC (**A**) and PMEC (**B**) differentiation protocols.
683 Endothelial cell (CD144+CD140a-) were FACS sorted on days 6 and day 8 for bulk
684 RNA-seq. ACTA: activin-A. CHIR: CHIR99021. pPSM/aPSM: posterior/anterior
685 presomitic mesoderm. LPM: lateral plate mesoderm. (**C**) Flow cytometry analysis of
686 CD140a and CD144 expression on day 6 and day 8 of CMEC and PMEC
687 differentiation. (**D**) Quantification of VEC (CD144)+CD140a- cells on day 6 and day 8

688 of CMEC and PMEC differentiation. Error bars represented standard deviations
689 calculated from five to six independent differentiations. (**E**) PCA analysis of ECs sorted
690 on day 6 and 8 of the CMEC or PMEC protocol. (**F**) GO term enrichment analysis for
691 DEGs between CMECs and PMECs on day 6 of differentiation. Complete list of GO
692 terms can be found in Table S2. Color represents the $p_{adjusted}$ of enrichment analysis
693 and dot size represents the count of genes mapped to the GO term. (**G**) Normalized
694 gene expression levels (RPKM) of cardiac and skeletal related genes in CMECs and
695 PMECs on day 6 and 8.
696
697 **Figure 2. Single-cell RNA sequencing analysis of ECs differentiated from**
698 **cardiac and paraxial mesoderm**
699 (**A-B**) Schematic overview of CMEC (**A**) and PMEC (**B**) differentiation protocols until
700 day 6. Cells were collected for scRNA-seq on day 6. ACTA: activin-A. CHIR:
701 CHIR99021. pPSM/aPSM: posterior/anterior presomitic mesoderm. LPM: lateral plate
702 mesoderm. (**C**) scRNA-seq of CMEC differentiation on day 6 (PAGA plot). Three
703 clusters of cells, indicated by color, were identified. (**D**) PAGA plots show expression
704 of *MESP1, ISL1, SMARCD3, CDH5, MYL4* on day 6 of CMEC differentiation. Color
705 represents log transformed expression. (**E**) Diffusion pseudotime analysis of CMEC
706 differentiation on day 6. (**F**) scRNA-seq of PMEC differentiation on day 6 (PAGA plot).
707 Three clusters of cells, indicated by color, were identified. (**G**) PAGA plots show
708 expression *PAX3, EYA1, FOXC1, CDH5, PPRX1* on day 6 of CMEC differentiation.
709 Color represents log transformed expression. (**H**) Diffusion pseudotime analysis of
710 PMEC differentiation on day 6.
711
712 **Figure 3. hiPSC-ECs acquired organ-specific signatures in a cardiac**
713 **microenvironment**
714 (**A**) Generation of cardiac MTs from hiPSC-CMs, hiPSC-CFs and hiPSC-ECs. CMECs
715 and PMECs were used for CM_MTs and PM_MTs respectively. MTs were collected
716 after 21 days for scRNAseq. (**B**) scRNAseq data of CM_MTs (left) and PM_MTs (right)
717 were visualized using PAGA. Three clusters of cells were identified in both datasets.
718 (**C**) Volcano plot showing fold changes and p-values of differential expression tests
719 between CMECs_day 6 and CMECs_MTs (left), or PMECs_day 6 and PMECs_MTs
720 (right). Representative intra-myocardial and endocardial markers that are differentially

721 expressed ($p_{adjusted}$<0.05) are highlighted in red and green, respectively. (**D-F**) Violin
722 plots of gene expression in PMECs_ day 6, CMECs_day6, CMECs_MT and
723 PMECs_MT for representative Intra-myocardial EC markers. Asterisks indicate
724 significance level of differential gene expression tests between the respective
725 populations. ns: p>0.05; * p <= 0.05; ** p<= 1e-10; *** p<= 1e-100; **** p<= 1e-200.
726 The clusters with higher expression value were labeled. ne: not expressed (0 counts)
727 in >85% of cells in both groups.
728
729 **Figure 4. CMECs and PMECs acquired intramyocardial identity in cardiac**
730 **microenvironment**
731 (**A-B**) Low-dimensional representation (UMAP) of the human fetal heart data set (Asp
732 et al., 2019) integrated with the CM_MTs (**A, C**) or PM_MTs (**B, D**) dataset. EC clusters
733 are marked with squares. Cell clusters are indicated by color. Cells in fetal heart
734 dataset are presented with dots and cells in MTs datasets are presented with contour
735 lines. (**C-D**) Zoom-ins of the EC clusters marked in (**A-B**). (**E**) Annotation of CM_MT
736 and PM_MT cells based on nearest neighbors in the *in vivo* dataset. Cells from
737 CM_MTs and PM_MTs are outlined with a green or violet contour, respectively. (**F**)
738 Jaccard similarity to intramyocardial ECs from the human fetal heart dataset was
739 calculated for each indicated group of genes. CM_MTs (ECs): specific markers of
740 cluster CMECs within the CM_MT dataset; PM_MTs (ECs): specific markers of cluster
741 PMECs within the PM_MT dataset; Up in CMECs_MT: DEGs that are higher in
742 CMECs_MT compared to CMECs_day 6; Up in PMECs_MT: DEGs that are higher in
743 PMECs_MT compared to PMECs_day 6; Up in P2 CMECs: DEGs that are higher in
744 passage two CMECs compared to CMECs_day 6. (**G**) Venn diagram shows numbers
745 and overlap of DEGs ($p_{adjusted}$<0.05 and fold-change > 1.5) between CMECs and
746 PMECs from day 6 (in red) and MTs (in blue). (**H**) PCA plot of different EC populations
747 in scRNAseq (triangle and diamond) and bulk RNA-seq (circle) datasets. Average
748 expression values of all cells in the cluster were used for the scRNA-seq data.
749
750 **Figure S1. Characterization of PMEC differentiation using**
751 **MSGN1^{mCherry}PAX3^{Venus} dual reporter line**
752 (**A**) Targeting constructs used to generate PAX3-Venus and MSGN1-mCherry hiPSC
753 reporter line. (**B**) Flow cytometry analysis of PAX3^{Venus} and MSGN1^{mCherry} expression

754 on day 2, 3, 5, 6 and 8 of PMEC differentiation. (**C-D**) Quantification of mCherry+ (**C**)
755 and Venus+ (**D**) cells in the total population by flow cytometry on day 2, 3, 5, 6 and 8.
756 (**E**) Representative fluorescence image of PAX3^{Venus} expression on day 5 of PMEC
757 differentiation. Scale bar: 200 μm. (**F**) Quantification of *TBXT, MIXL1, MESP1,*
758 *GATA4, NKX2-5, MSGN1, TBX6* and *PAX3* expression by qPCR on day 0, 2, 5 and 8
759 of CMEC (green) and PMEC (purple) differentiation.
760
761 **Figure S2. Quality control of scRNAseq datasets**
762 (**A-B**) Distribution of the number of detected genes (**A**) and total expression (**B**) in
763 each cell of the scRNAseq datasets. The dotted blue lines indicate quality control
764 thresholds. Two different batches are labelled with different colors. (**C**) Two different
765 batches of cells collected for each scRNAseq dataset were visualized with PAGA.
766 (**D**) scRNAseq data of CMECs on day 6 is visualized using PAGA. Five cell clusters
767 were identified and labelled with different colors. (**E**) Expression of pluripotency genes
768 *POU5F1* and *NANOG* in the CMECa dataset on day 6 is shown in PAGA plot. Color
769 represents log transformed expression. (**F-G**) scRNAseq data of CM_MTs (**F**) and
770 PM_MTs (**G**) were visualized using PAGA. Four cell clusters were identified. Clusters
771 labelled with "Other" were excluded from downstream analysis. (**H**) Boxplot of G2M
772 phase-score in individual clusters of each dataset.
773
774 **Figure S3. scRNAseq analysis of CMEC and PMEC datasets on day 6**
775 (**A**) Volcano plots showing fold changes and p-values of differential expression tests
776 between individual CMEC clusters and all other cells. Representative significantly up-
777 regulated genes ($p_{adjusted} < 0.05$ & fold-change > 1.2) are labelled in red. (**B**) *MESP1*,
778 *SMARCD3*, *KDR*, *CDH5*, *MYL4* and *NKX2*-5 expression (log transformed) in three
779 clusters of the CMEC dataset on day 6. (**C**) Volcano plots showing fold-changes and
780 p-values of differential expression tests between individual PMEC clusters and all
781 other cells. Representative significantly up-regulated genes ($p_{adjusted}<0.05$ & fold
782 change > 1.2) are labelled in red. (**D**) *PAX3*, *MEOX1*, *CD34*, *CDH5*, *HAND1* and
783 *PRRX1* expression (log transformed) in three clusters of PMEC dataset on day 6.
784
785 **Figure S4. Re-analysis of a published scRNAseq dataset to identify organ**
786 **specific signatures of human fetal heart ECs**

(**A**) Low-dimensional representation (UMAP) of scRNAseq of the human fetal heart (Asp et al., 2019). 14 cell clusters were identified and named based on the original publication, except for two EC clusters: intramyocardial ECs and endocardium. (**B**) Volcano plot showing fold changes and p-values for differential expression tests between intra-myocardial ECs and endocardium in the data set shown in (**A**). Representative differentially expressed genes ($p_{adjusted}$<0.05) that are known as intramyocardial and endocardial markers are labelled in red and green respectively. (**C-D**) Low-dimensional representation (UMAP) of scRNAseq of the human fetal heart (Asp et al., 2019). Log-transformed expression of representative intramyocardial EC markers (**C**) and endocardium markers (**D**) is indicated by color.

Figure S5. Comparison of organ-specific signatures of hiPSC-ECs on day 6 with ECs in MTs

(**A-C**) Differential expression test between clusters CMECs_day 6 and CMECs_MT (**A**), PMECs_ day 6 and PMECs_MT (**B**), CMECs_MT and PMECs_MT (**C**) for representative endocardial EC markers. ns: p>0.05; * p <=0.05; ** p<= 1e-10; *** p<= 1e-100; **** p<= 1e-200. Clusters with higher expression value were indicated with stars. ne: not expressed (0 counts) in >85% of cells in both groups.

References

Aird WC. 2012. Endothelial Cell Heterogeneity. *Cold Spring Harbor Perspectives in Medicine* 2:a006429–a006429. doi:10.1101/cshperspect.a006429

Asp M, Giacomello S, Larsson L, Wu C, Fürth D, Qian X, Wärdell E, Custodio J, Reimegård J, Salmén F, Österholm C, Ståhl PL, Sundström E, Åkesson E, Bergmann O, Bienko M, Månsson-Broberg A, Nilsson M, Sylvén C, Lundeberg J. 2019. A Spatiotemporal Organ-Wide Gene Expression and Cell Atlas of the Developing Human Heart. *Cell* 179:1647-1660.e19. doi:10.1016/j.cell.2019.11.025

Breitkopf-Heinlein K, Meyer C, König C, Gaitantzi H, Addante A, Thomas M, Wiercinska E, Cai C, Li Q, Wan F, Hellerbrand C, Valous NA, Hahnel M, Ehlting

818 C, Bode JG, Müller-Bohl S, Klingmüller U, Altenöder J, Ilkavets I, Goumans M-J,
819 Hawinkels LJAC, Lee S-J, Wieland M, Mogler C, Ebert MP, Herrera B, Augustin
820 H, Sánchez A, Dooley S, Dijke P ten. 2017. BMP-9 interferes with liver
821 regeneration and promotes liver fibrosis. *Gut* 66:939. doi:10.1136/gutjnl-2016-
822 313314

823 Brink SC van den, Sage F, Vértesy Á, Spanjaard B, Peterson-Maduro J, Baron CS,
824 Robin C, Oudenaarden A van. 2017. Single-cell sequencing reveals dissociation-
825 induced gene expression in tissue subpopulations. *Nat Methods*, Nature methods
826 14:935–936. doi:10.1038/nmeth.4437

827 Brutsaert DL. 2003. Cardiac Endothelial-Myocardial Signaling: Its Role in Cardiac
828 Growth, Contractile Performance, and Rhythmicity. *Physiological Reviews* 83:59–
829 115. doi:10.1152/physrev.00017.2002

830 Campostrini G, Windt LM, Meer BJ van, Bellin M, Mummery CL. 2021. Cardiac
831 Tissues From Stem Cells. *Circ Res* 128:775–801.
832 doi:10.1161/circresaha.121.318183

833 Cao X, Mircea M, Yakala GK, Hil FE van den, Brescia M, Mei H, Mummery CL,
834 Semrau S, Orlova VV. 2022. ETV2 upregulation marks the specification of early
835 cardiomyocytes and endothelial cells during co-differentiation. *bioRxiv*
836 2022.11.15.516686. doi:10.1101/2022.11.15.516686

837 Costa M, Dottori M, Sourris K, Jamshidi P, Hatzistavrou T, Davis R, Azzola L,
838 Jackson S, Lim SM, Pera M, Elefanty AG, Stanley EG. 2007. A method for
839 genetic modification of human embryonic stem cells using electroporation. *Nat*
840 *Protoc* 2:792–796. doi:10.1038/nprot.2007.105

841 Ditadi A, Sturgeon CM, Tober J, Awong G, Kennedy M, Yzaguirre AD, Azzola L, Ng
842 ES, Stanley EG, French DL, Cheng X, Gadue P, Speck NA, Elefanty AG, Keller
843 G. 2015. Human definitive haemogenic endothelium and arterial vascular
844 endothelium represent distinct lineages. *Nature Cell Biology* 17:580–591.
845 doi:10.1038/ncb3161

846 Drakhlis L, Biswanath S, Farr C-M, Lupanow V, Teske J, Ritzenhoff K, Franke A,
847 Manstein F, Bolesani E, Kempf H, Liebscher S, Schenke-Layland K, Hegermann
848 J, Nolte L, Meyer H, Roche J de la, Thiemann S, Wahl-Schott C, Martin U,
849 Zweigerdt R. 2021. Human heart-forming organoids recapitulate early heart and
850 foregut development. *Nat Biotechnol* 1–10. doi:10.1038/s41587-021-00815-9

851 Gage BK, Liu JC, Innes BT, MacParland SA, McGilvray ID, Bader GD, Keller GM.
852 2020. Generation of Functional Liver Sinusoidal Endothelial Cells from Human
853 Pluripotent Stem-Cell-Derived Venous Angioblasts. *Cell Stem Cell* 27:254-269.e9.
854 doi:10.1016/j.stem.2020.06.007

855 Géraud C, Koch P-S, Zierow J, Klapproth K, Busch K, Olsavszky V, Leibing T,
856 Demory A, Ulbrich F, Diett M, Singh S, Sticht C, Breitkopf-Heinlein K, Richter K,
857 Karppinen S-M, Pihlajaniemi T, Arnold B, Rodewald H-R, Augustin HG,
858 Schledzewski K, Goerdt S. 2017. GATA4-dependent organ-specific endothelial
859 differentiation controls liver development and embryonic hematopoiesis. *J Clin*
860 *Invest* 127:1099–1114. doi:10.1172/jci90086

861 Giacomelli E, Bellin M, Sala L, Meer BJ van, Tertoolen LGJ, Orlova VV, Mummery
862 CL. 2017. Three-dimensional cardiac microtissues composed of cardiomyocytes
863 and endothelial cells co-differentiated from human pluripotent stem cells.
864 *Development* 144:1008–1017. doi:10.1242/dev.143438

865 Giacomelli E, Meraviglia V, Campostrini G, Cochrane A, Cao X, Helden RWJ van,
866 Garcia AK, Mircea M, Kostidis S, Davis RP, Meer BJ van, Jost CR, Koster AJ, Mei
867 H, Míguez DG, Mulder AA, Ledesma-Terrón M, Pompilio G, Sala L, Salvatori
868 DCF, Slieker RC, Sommariva E, Vries AAF de, Giera M, Semrau S, Tertoolen
869 LGJ, Orlova VV, Bellin M, Mummery CL. 2020. Human-iPSC-Derived Cardiac
870 Stromal Cells Enhance Maturation in 3D Cardiac Microtissues and Reveal Non-
871 cardiomyocyte Contributions to Heart Disease. *Cell Stem Cell* 26:862-879.e11.
872 doi:10.1016/j.stem.2020.05.004

873 Giotti B, Joshi A, Freeman TC. 2017. Meta-analysis reveals conserved cell cycle
874 transcriptional network across multiple human cell types. *Bmc Genomics* 18:30.
875 doi:10.1186/s12864-016-3435-2

876 Gómez-Salinero JM, Izzo F, Lin Y, Houghton S, Itkin T, Geng F, Bram Y, Adelson
877 RP, Lu TM, Inghirami G, Xiang JZ, Lis R, Redmond D, Schreiner R, Rabbany SY,
878 Landau DA, Schwartz RE, Rafii S. 2022. Specification of fetal liver endothelial
879 progenitors to functional zonated adult sinusoids requires c-Maf induction. *Cell*
880 *Stem Cell* 29:593-609.e7. doi:10.1016/j.stem.2022.03.002

881 Haghverdi L, Büttner M, Wolf FA, Buettner F, Theis FJ. 2016. Diffusion pseudotime
882 robustly reconstructs lineage branching. *Nat Methods* 13:845–848.
883 doi:10.1038/nmeth.3971

884 Hansen KD, Irizarry RA, Wu Z. 2012. Removing technical variability in RNA-seq data
885 using conditional quantile normalization. *Biostat Oxf Engl*, Biostatistics 13:204–16.
886 doi:10.1093/biostatistics/kxr054

887 He L, Zhou B. 2018. The Development and Regeneration of Coronary Arteries. *Curr*
888 *Cardiol Rep* 20:54. doi:10.1007/s11886-018-0999-2

889 Hofbauer P, Jahnel SM, Mendjan S. 2021a. In vitro models of the human heart.
890 *Development* 148. doi:10.1242/dev.199672

891 Hofbauer P, Jahnel SM, Papai N, Giesshammer M, Deyett A, Schmidt C, Penc M,
892 Tavernini K, Grdseloff N, Meledeth C, Ginistrelli LC, Ctortecka C, Šalic Š,
893 Novatchkova M, Mendjan S. 2021b. Cardioids reveal self-organizing principles of
894 human cardiogenesis. *Cell*. doi:10.1016/j.cell.2021.04.034

895 Iso T, Maeda K, Hanaoka H, Suga T, Goto K, Syamsunarno MRAA, Hishiki T,
896 Nagahata Y, Matsui H, Arai M, Yamaguchi A, Abumrad NA, Sano M, Suematsu
897 M, Endo K, Hotamisligil GS, Kurabayashi M. 2018. Capillary Endothelial Fatty
898 Acid Binding Proteins 4 and 5 Play a Critical Role in Fatty Acid Uptake in Heart
899 and Skeletal Muscle. *Arteriosclerosis Thrombosis Vasc Biology* 33:2549–2557.
900 doi:10.1161/atvbaha.113.301588

901 Lagha M, Brunelli S, Messina G, Cumano A, Kume T, Relaix F, Buckingham ME.
902 2009. Pax3:Foxc2 Reciprocal Repression in the Somite Modulates Muscular
903 versus Vascular Cell Fate Choice in Multipotent Progenitors. *Developmental Cell*
904 17:892–899. doi:10.1016/j.devcel.2009.10.021

905 Lenti E, Genovese L, Bianchessi S, Maurizio A, Sain SB, Lillo A di, Mattavelli G,
906 Harel I, Bernassola F, Hehlgans T, Pfeffer K, Crosti M, Abrignani S, Evans SM,
907 Sitia G, Guimarães-Camboa N, Russo V, Pavert SA van de, Garcia-Manteiga JM,
908 Brendolan A. 2022. Fate mapping and scRNA sequencing reveal origin and
909 diversity of lymph node stromal precursors. *Immunity* 55:606-622.e6.
910 doi:10.1016/j.immuni.2022.03.002

911 Lewis-Israeli YR, Wasserman AH, Gabalski MA, Volmert BD, Ming Y, Ball KA, Yang
912 W, Zou J, Ni G, Pajares N, Chatzistavrou X, Li W, Zhou C, Aguirre A. 2021. Self-
913 assembling human heart organoids for the modeling of cardiac development and
914 congenital heart disease. *Nat Commun* 12:5142. doi:10.1038/s41467-021-25329-
915 5

916 Lioux G, Liu X, Temiño S, Oxendine M, Ayala E, Ortega S, Kelly RG, Oliver G,
917 Torres M. 2020. A Second Heart Field-Derived Vasculogenic Niche Contributes to
918 Cardiac Lymphatics. *Dev Cell* 52:350-363.e6. doi:10.1016/j.devcel.2019.12.006

919 Loh KM, Chen A, Koh PW, Deng TZ, Sinha R, Tsai JM, Barkal AA, Shen KY, Jain R,
920 Morganti RM, Shyh-Chang N, Fernhoff NB, George BM, Wernig G, Salomon
921 REA, Chen Z, Vogel H, Epstein JA, Kundaje A, Talbot WS, Beachy PA, Ang LT,
922 Weissman IL. 2016. Mapping the Pairwise Choices Leading from Pluripotency to
923 Human Bone, Heart, and Other Mesoderm Cell Types. *Cell* 166:451–467.
924 doi:10.1016/j.cell.2016.06.011

925 Lun ATL, Bach K, Marioni JC. 2016. Pooling across cells to normalize single-cell
926 RNA sequencing data with many zero counts. *Genome Biol*, Genome biology
927 17:75. doi:10.1186/s13059-016-0947-7

928 Lupu I-E, Kirschnick N, Weischer S, Martinez-Corral I, Forrow A, Lahmann I, Riley
929 PR, Zobel T, Makinen T, Kiefer F, Stone OA. 2022. Direct specification of

930 lymphatic endothelium from non-venous angioblasts. *Biorxiv* 2022.05.11.491403.
931 doi:10.1101/2022.05.11.491403

932 Martin M. 2011. Cutadapt removes adapter sequences from high-throughput
933 sequencing reads. *Embnet J*, EMBnet.journal 17:10–12. doi:10.14806/ej.17.1.200

934 Mayeuf-Louchart A, Montarras D, Bodin C, Kume T, Vincent SD, Buckingham M.
935 2016. Endothelial cell specification in the somite is compromised in Pax3-positive
936 progenitors of Foxc1/2 conditional mutants, with loss of forelimb myogenesis.
937 *Development* 1–26. doi:10.1242/dev.128017

938 McCracken IR, Dobie R, Bennett M, Passi R, Beqqali A, Henderson NC, Mountford
939 JC, Riley PR, Ponting CP, Smart N, Brittan M, Baker AH. 2022. Mapping the
940 developing human cardiac endothelium at single cell resolution identifies MECOM
941 as a regulator of arteriovenous gene expression. *Cardiovasc Res* cvac023-.
942 doi:10.1093/cvr/cvac023

943 Miao Y, Tian L, Martin M, Paige SL, Galdos FX, Li J, Klein A, Zhang H, Ma N, Wei Y,
944 Stewart M, Lee S, Moonen J-R, Zhang B, Grossfeld P, Mital S, Chitayat D, Wu
945 JC, Rabinovitch M, Nelson TJ, Nie S, Wu SM, Gu M. 2020. Intrinsic Endocardial
946 Defects Contribute to Hypoplastic Left Heart Syndrome. *Cell Stem Cell* 27:574-
947 589.e8. doi:10.1016/j.stem.2020.07.015

948 Mikryukov AA, Mazine A, Wei B, Yang D, Miao Y, Gu M, Keller GM. 2021. BMP10
949 Signaling Promotes the Development of Endocardial Cells from Human
950 Pluripotent Stem Cell-Derived Cardiovascular Progenitors. *Cell Stem Cell* 28.
951 doi:10.1016/j.stem.2020.10.003

952 Milgrom-Hoffman M, Harrelson Z, Ferrara N, Zelzer E, Evans SM, Tzahor E. 2011.
953 The heart endocardium is derived from vascular endothelial progenitors.
954 *Development* 138:4777–4787. doi:10.1242/dev.061192

955 Ng ES, Azzola L, Bruveris FF, Calvanese V, Phipson B, Vlahos K, Hirst C, Jokubaitis
956 VJ, Yu QC, Maksimovic J, Liebscher S, Januar V, Zhang Z, Williams B,
957 Conscience A, Durnall J, Jackson S, Costa M, Elliott D, Haylock DN, Nilsson SK,

958 Saffery R, Schenke-Layland K, Oshlack A, Mikkola HKA, Stanley EG, Elefanty
959 AG. 2016. Differentiation of human embryonic stem cells to HOXA+ hemogenic
960 vasculature that resembles the aorta-gonad-mesonephros. *Nature Biotechnology*
961 34:1168–1179. doi:10.1038/nbt.3702

962 Ng ES, Davis R, Stanley EG, Elefanty AG. 2008. A protocol describing the use of a
963 recombinant protein-based, animal product-free medium (APEL) for human
964 embryonic stem cell differentiation as spin embryoid bodies. *Nature Protocols*
965 3:768–776. doi:10.1038/nprot.2008.42

966 Pardanaud L, Luton D, Prigent M, Bourcheix LM, Catala M, Dieterlen-Lievre F. 1996.
967 Two distinct endothelial lineages in ontogeny, one of them related to hemopoiesis.
968 *Development* 122:1363–1371. doi:10.1242/dev.122.5.1363

969 Phansalkar R, Krieger J, Zhao M, Kolluru SS, Jones RC, Quake SR, Weissman I,
970 Bernstein D, Winn VD, D'Amato G, Red-Horse K. 2021. Coronary blood vessels
971 from distinct origins converge to equivalent states during mouse and human
972 development. *Elife* 10:e70246. doi:10.7554/elife.70246

973 Qu X, Harmelink C, Baldwin HS. 2022. Endocardial-Myocardial Interactions During
974 Early Cardiac Differentiation and Trabeculation. *Frontiers Cardiovasc Medicine*
975 9:857581. doi:10.3389/fcvm.2022.857581

976 Ritchie ME, Phipson B, Wu D, Hu Y, Law CW, Shi W, Smyth GK. 2015. limma
977 powers differential expression analyses for RNA-sequencing and microarray
978 studies. *Nucleic Acids Res* 43:e47. doi:10.1093/nar/gkv007

979 Robinson MD, McCarthy DJ, Smyth GK. 2009. edgeR: a Bioconductor package for
980 differential expression analysis of digital gene expression data. *Bioinform Oxf*
981 *Engl*, Bioinformatics (Oxford, England) 26:139–40.
982 doi:10.1093/bioinformatics/btp616

983 Rostovskaya M, Fu J, Obst M, Baer I, Weidlich S, Wang H, Smith AJH,
984 Anastassiadis K, Stewart AF. 2012. Transposon-mediated BAC transgenesis in
985 human ES cells. *Nucleic Acids Res* 40:e150–e150. doi:10.1093/nar/gks643

986 Scialdone A, Natarajan KN, Saraiva LR, Proserpio V, Teichmann SA, Stegle O,
987 Marioni JC, Buettner F. 2015. Computational assignment of cell-cycle stage from
988 single-cell transcriptome data. *Methods San Diego Calif* 85:54–61.
989 doi:10.1016/j.ymeth.2015.06.021

990 Sharma B, Chang A, Red-Horse K. 2017a. Coronary Artery Development: Progenitor
991 Cells and Differentiation Pathways. *Annual Review of Physiology* 79:1–19.
992 doi:10.1146/annurev-physiol-022516-033953

993 Sharma B, Ho L, Ford GH, Chen HI, Goldstone AB, Woo YJ, Quertermous T,
994 Reversade B, Red-Horse K. 2017b. Alternative Progenitor Cells Compensate to
995 Rebuild the Coronary Vasculature in Elabela- and Apj-Deficient Hearts.
996 *Developmental Cell* 42:1–16. doi:10.1016/j.devcel.2017.08.008

997 Silva AC, Matthys OB, Joy DA, Kauss MA, Natarajan V, Lai MH, Turaga D, Blair AP,
998 Alexanian M, Bruneau BG, McDevitt TC. 2021. Co-emergence of cardiac and gut
999 tissues promotes cardiomyocyte maturation within human iPSC-derived
1000 organoids. *Cell Stem Cell* 28:2137-2152.e6. doi:10.1016/j.stem.2021.11.007

1001 Stone OA, Stainier DYR. 2019. Paraxial Mesoderm Is the Major Source of Lymphatic
1002 Endothelium. *Dev Cell* 50:247-255.e3. doi:10.1016/j.devcel.2019.04.034

1003 Thomas D, Choi S, Alamana C, Parker KK, Wu JC. 2022. Cellular and Engineered
1004 Organoids for Cardiovascular Models. *Circ Res* 130:1780–1802.
1005 doi:10.1161/circresaha.122.320305

1006 Tian X, Zhou B. 2022. Coronary vessel formation in development and regeneration:
1007 origins and mechanisms. *J Mol Cell Cardiol* 167:67–82.
1008 doi:10.1016/j.yjmcc.2022.03.009

1009 Uenishi G, Theisen D, Lee J-H, Kumar A, Raymond M, Vodyanik M, Swanson S,
1010 Stewart R, Thomson J, Slukvin I. 2014. Tenascin C promotes hematoendothelial
1011 development and T lymphoid commitment from human pluripotent stem cells in
1012 chemically defined conditions. *STEMCR* 3:1073–1084.
1013 doi:10.1016/j.stemcr.2014.09.014

1014 Whitfield ML, George LK, Grant GD, Perou CM. 2006. Common markers of
1015 proliferation. *Nat Rev Cancer*, Nature reviews. Cancer 6:99–106.
1016 doi:10.1038/nrc1802

1017 Wolf FA, Hamey FK, Plass M, Solana J, Dahlin JS, Göttgens B, Rajewsky N, Simon
1018 L, Theis FJ. 2019. PAGA: graph abstraction reconciles clustering with trajectory
1019 inference through a topology preserving map of single cells. *Genome Biol* 20:59.
1020 doi:10.1186/s13059-019-1663-x

1021 Wu TD, Nacu S. 2010. Fast and SNP-tolerant detection of complex variants and
1022 splicing in short reads. *Bioinform Oxf Engl*, Bioinformatics (Oxford, England)
1023 26:873–81. doi:10.1093/bioinformatics/btq057

1024 Wu TD, Watanabe CK. 2005. GMAP: a genomic mapping and alignment program for
1025 mRNA and EST sequences. *Bioinformatics*, Bioinformatics (Oxford, England)
1026 21:1859–1875. doi:10.1093/bioinformatics/bti310

1027 Yates A, Akanni W, Amode MR, Barrell D, Billis K, Carvalho-Silva D, Cummins C,
1028 Clapham P, Fitzgerald S, Gil L, Girón CG, Gordon L, Hourlier T, Hunt SE,
1029 Janacek SH, Johnson N, Juettemann T, Keenan S, Lavidas I, Martin FJ, Maurel
1030 T, McLaren W, Murphy DN, Nag R, Nuhn M, Parker A, Patricio M, Pignatelli M,
1031 Rahtz M, Riat HS, Sheppard D, Taylor K, Thormann A, Vullo A, Wilder SP,
1032 Zadissa A, Birney E, Harrow J, Muffato M, Perry E, Ruffier M, Spudich G,
1033 Trevanion SJ, Cunningham F, Aken BL, Zerbino DR, Flicek P. 2015. Ensembl
1034 2016. *Nucleic Acids Res*, Nucleic acids research 44:D710-6.
1035 doi:10.1093/nar/gkv1157

1036 Yu G, Wang L-G, Han Y, He Q-Y. 2012. clusterProfiler: an R Package for Comparing
1037 Biological Themes Among Gene Clusters. *Omics J Integr Biology*, OMICS: A
1038 Journal of Integrative Biology 16:284–287. doi:10.1089/omi.2011.0118

1039 Zhang H, Pu W, Li G, Huang X, He L, Tian X, Liu Q, Zhang L, Wu SM, Sucov HM,
1040 Zhou B. 2016a. Endocardium Minimally Contributes to Coronary Endothelium in
1041 the Embryonic Ventricular Free Walls. *Circulation Research* 118:1880–1893.
1042 doi:10.1161/circresaha.116.308749

1043 Zhang H, Pu W, Tian X, Huang X, He Lingjuan, Liu Q, Li Y, Zhang L, He Liang, Liu
1044 K, Gillich A, Zhou B. 2016b. Genetic lineage tracing identifies endocardial origin of
1045 liver vasculature. *Nature Genetics* 48:1–9. doi:10.1038/ng.3536

1046

Figure 1.

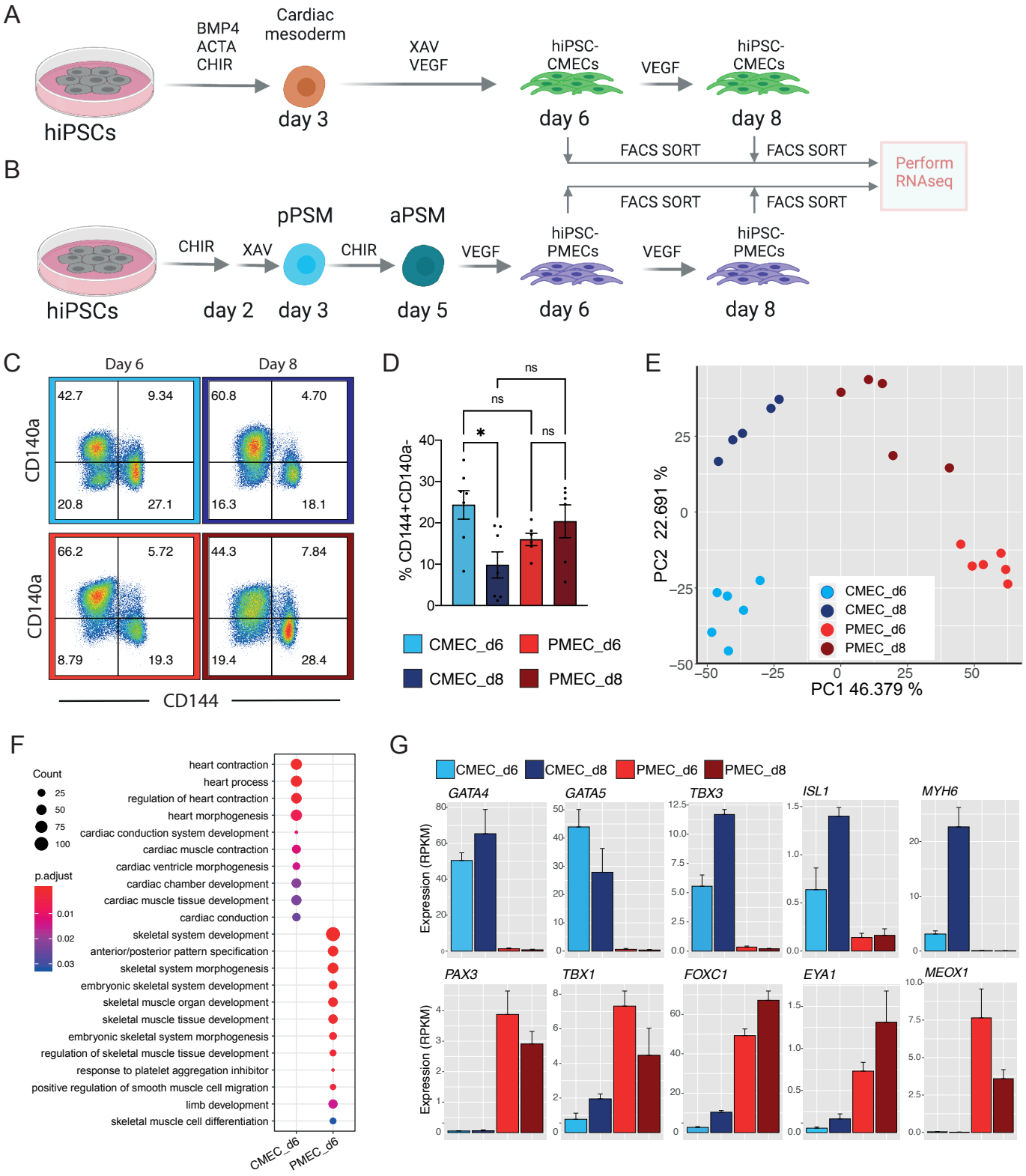
A
hiPSCs
BMP4
ACTA
CHIR
Cardiac mesoderm
day 3
XAV
VEGF
hiPSC-CMECs
day 6
VEGF
hiPSC-CMECs
day 8
FACS SORT
FACS SORT
Perform RNAseq
B
hiPSCs
CHIR
XAV
pPSM
CHIR
aPSM
VEGF
hiPSC-PMECs
VEGF
hiPSC-PMECs
FACS SORT
FACS SORT
day 2
day 3
day 5
day 6
day 8
C
Day 6
Day 8
CD140a
CD144
42.7
9.34
20.8
27.1
60.8
4.70
16.3
18.1
66.2
5.72
8.79
19.3
44.3
7.84
19.4
28.4
D
% CD144+CD140a-
ns
ns
ns
*
CMEC_d6
CMEC_d8
PMEC_d6
PMEC_d8
E
PC2 22.691 %
PC1 46.379 %
CMEC_d6
CMEC_d8
PMEC_d6
PMEC_d8
F
Count
25
50
75
100
p.adjust
0.01
0.02
0.03
heart contraction
heart process
regulation of heart contraction
heart morphogenesis
cardiac conduction system development
cardiac muscle contraction
cardiac ventricle morphogenesis
cardiac chamber development
cardiac muscle tissue development
cardiac conduction
skeletal system development
anterior/posterior pattern specification
skeletal system morphogenesis
embryonic skeletal system development
skeletal muscle organ development
skeletal muscle tissue development
embryonic skeletal system morphogenesis
regulation of skeletal muscle tissue development
response to platelet aggregation inhibitor
positive regulation of smooth muscle cell migration
limb development
skeletal muscle cell differentiation
CMEC_d6
PMEC_d6
G
CMEC_d6
CMEC_d8
PMEC_d6
PMEC_d8
GATA4
GATA5
TBX3
ISL1
MYH6
PAX3
TBX1
FOXC1
EYA1
MEOX1
Expression (RPKM)

Figure 2.

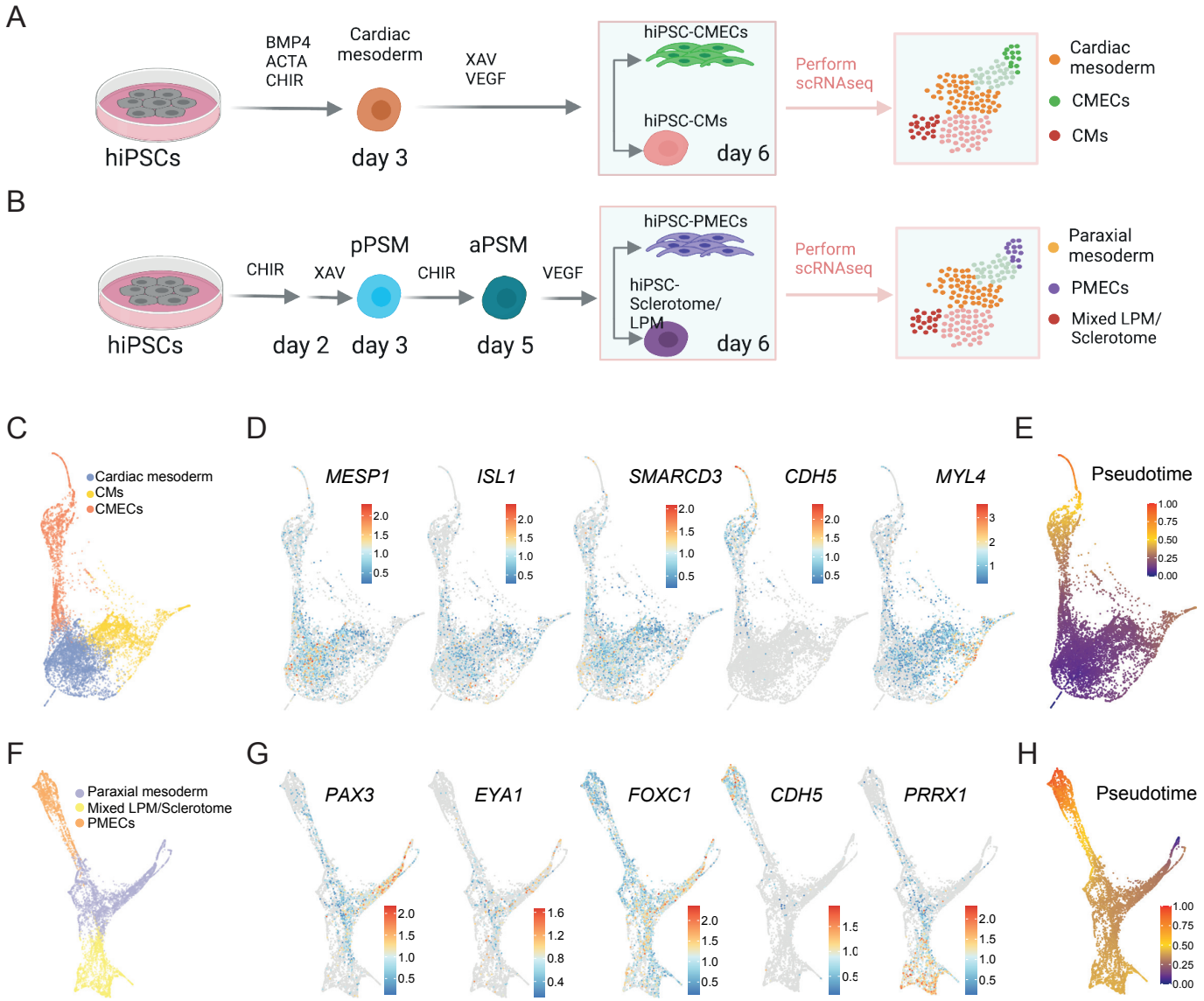
A
BMP4
ACTA
CHIR
Cardiac mesoderm
XAV
VEGF
hiPSCs
day 3
hiPSC-CMECs
hiPSC-CMs
day 6
Perform scRNAseq
Cardiac mesoderm
CMECs
CMs
B
CHIR
XAV
pPSM
CHIR
aPSM
VEGF
hiPSCs
day 2
day 3
day 5
hiPSC-PMECs
hiPSC-Sclerotome/LPM
day 6
Perform scRNAseq
Paraxial mesoderm
PMECs
Mixed LPM/Sclerotome
C
Cardiac mesoderm
CMs
CMECs
D
MESP1
ISL1
SMARCD3
CDH5
MYL4
E
Pseudotime
F
Paraxial mesoderm
Mixed LPM/Sclerotome
PMECs
G
PAX3
EYA1
FOXC1
CDH5
PRRX1
H
Pseudotime

Figure 3.

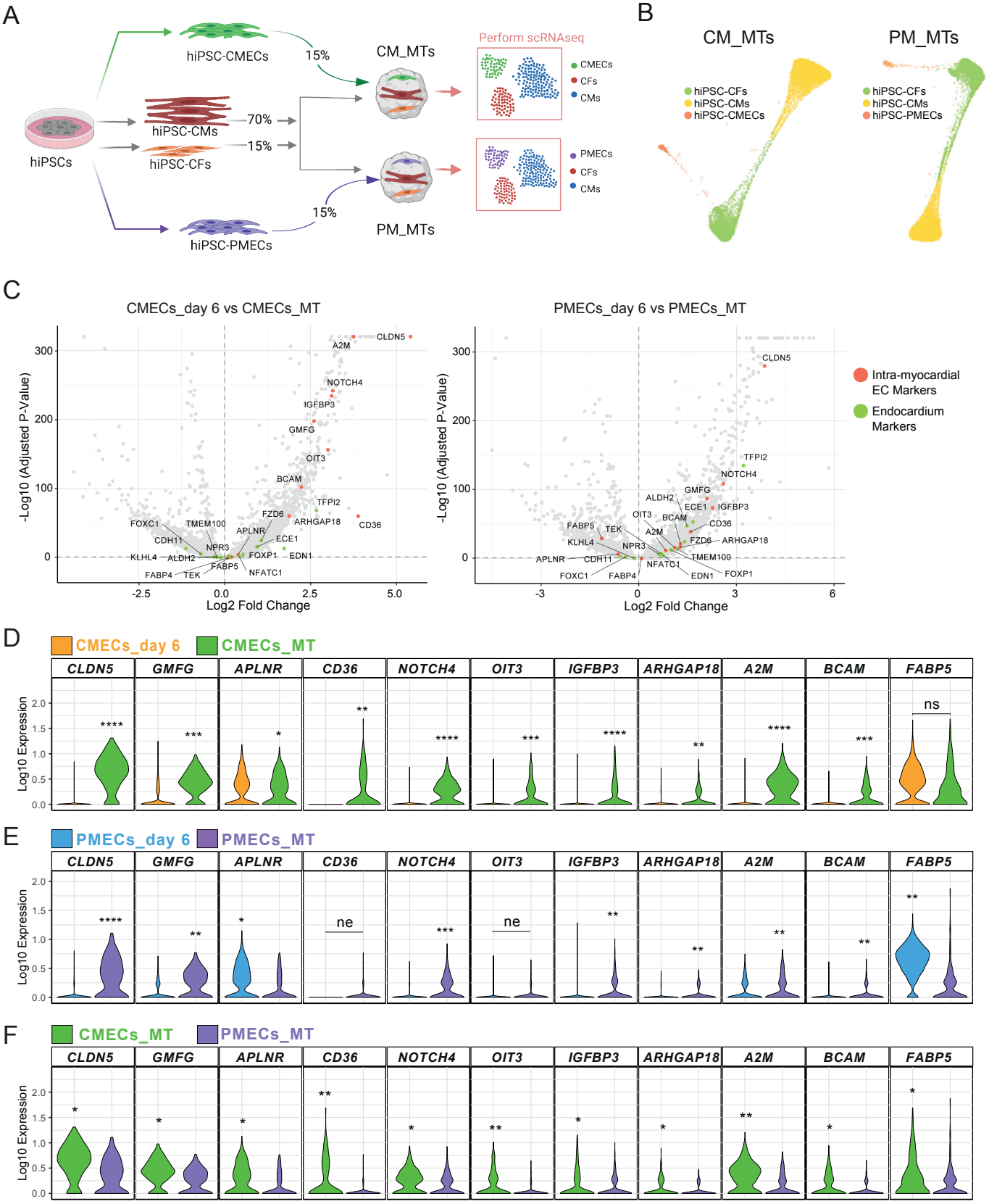
A
hiPSC-CMECs
15%
CM_MTs
Perform scRNAseq
CMECs
CFs
CMs
hiPSCs
hiPSC-CMs
70%
hiPSC-CFs
15%
PMECs
CFs
CMs
15%
hiPSC-PMECs
PM_MTs
B
CM_MTs
PM_MTs
hiPSC-CFs
hiPSC-CMs
hiPSC-CMECs
hiPSC-CFs
hiPSC-CMs
hiPSC-PMECs
C
CMECs_day 6 vs CMECs_MT
PMECs_day 6 vs PMECs_MT
-Log10 (Adjusted P-Value)
Log2 Fold Change
Intra-myocardial EC Markers
Endocardium Markers
D
CMECs_day 6
CMECs_MT
CLDN5
GMFG
APLNR
CD36
NOTCH4
OIT3
IGFBP3
ARHGAP18
A2M
BCAM
FABP5
Log10 Expression
ns
E
PMECs_day 6
PMECs_MT
ne
ne
F
CMECs_MT
PMECs_MT

Figure 4.

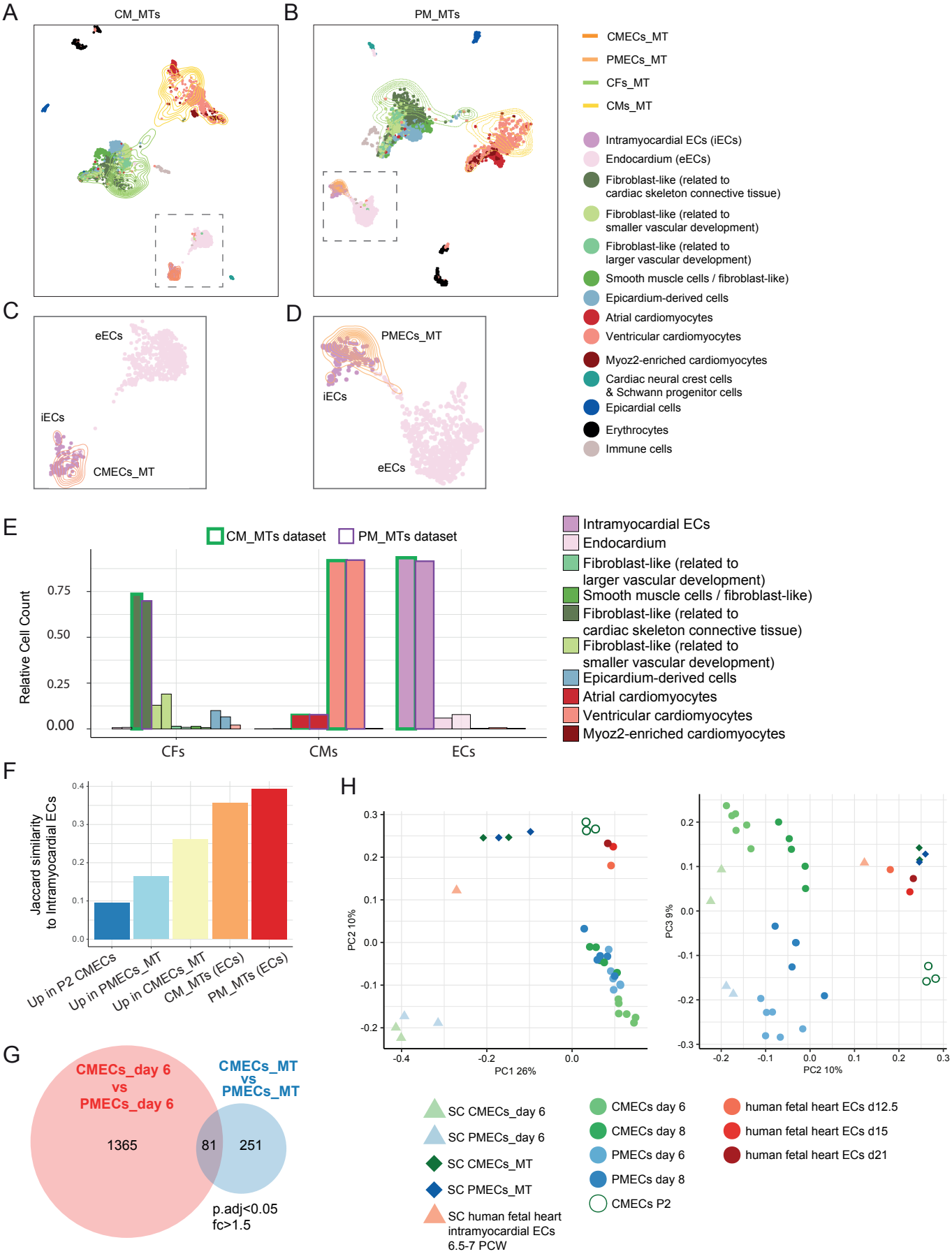
A
CM_MTs
B
PM_MTs
CMECs_MT
PMECs_MT
CFs_MT
CMs_MT
Intramyocardial ECs (iECs)
Endocardium (eECs)
Fibroblast-like (related to cardiac skeleton connective tissue)
Fibroblast-like (related to smaller vascular development)
Fibroblast-like (related to larger vascular development)
Smooth muscle cells / fibroblast-like)
Epicardium-derived cells
Atrial cardiomyocytes
Ventricular cardiomyocytes
Myoz2-enriched cardiomyocytes
Cardiac neural crest cells & Schwann progenitor cells
Epicardial cells
Erythrocytes
Immune cells
C
eECs
iECs
CMECs_MT
D
PMECs_MT
iECs
eECs
E
CM_MTs dataset
PM_MTs dataset
Relative Cell Count
0.75
0.50
0.25
0.00
CFs
CMs
ECs
Intramyocardial ECs
Endocardium
Fibroblast-like (related to larger vascular development)
Smooth muscle cells / fibroblast-like)
Fibroblast-like (related to cardiac skeleton connective tissue)
Fibroblast-like (related to smaller vascular development)
Epicardium-derived cells
Atrial cardiomyocytes
Ventricular cardiomyocytes
Myoz2-enriched cardiomyocytes
F
Jaccard similarity to Intramyocardial ECs
0.4
0.3
0.2
0.1
0.0
Up in P2 CMECs
Up in PMECs_MT
Up in CMECs_MT
CM_MTs (ECs)
PM_MTs (ECs)
G
CMECs_day 6 vs PMECs_day 6
CMECs_MT vs PMECs_MT
1365
81
251
p.adj<0.05
fc>1.5
H
PC2 10%
PC1 26%
PC3 9%
PC2 10%
SC CMECs_day 6
SC PMECs_day 6
SC CMECs_MT
SC PMECs_MT
SC human fetal heart intramyocardial ECs 6.5-7 PCW
CMECs day 6
CMECs day 8
PMECs day 6
PMECs day 8
CMECs P2
human fetal heart ECs d12.5
human fetal heart ECs d15
human fetal heart ECs d21

Figure S1.

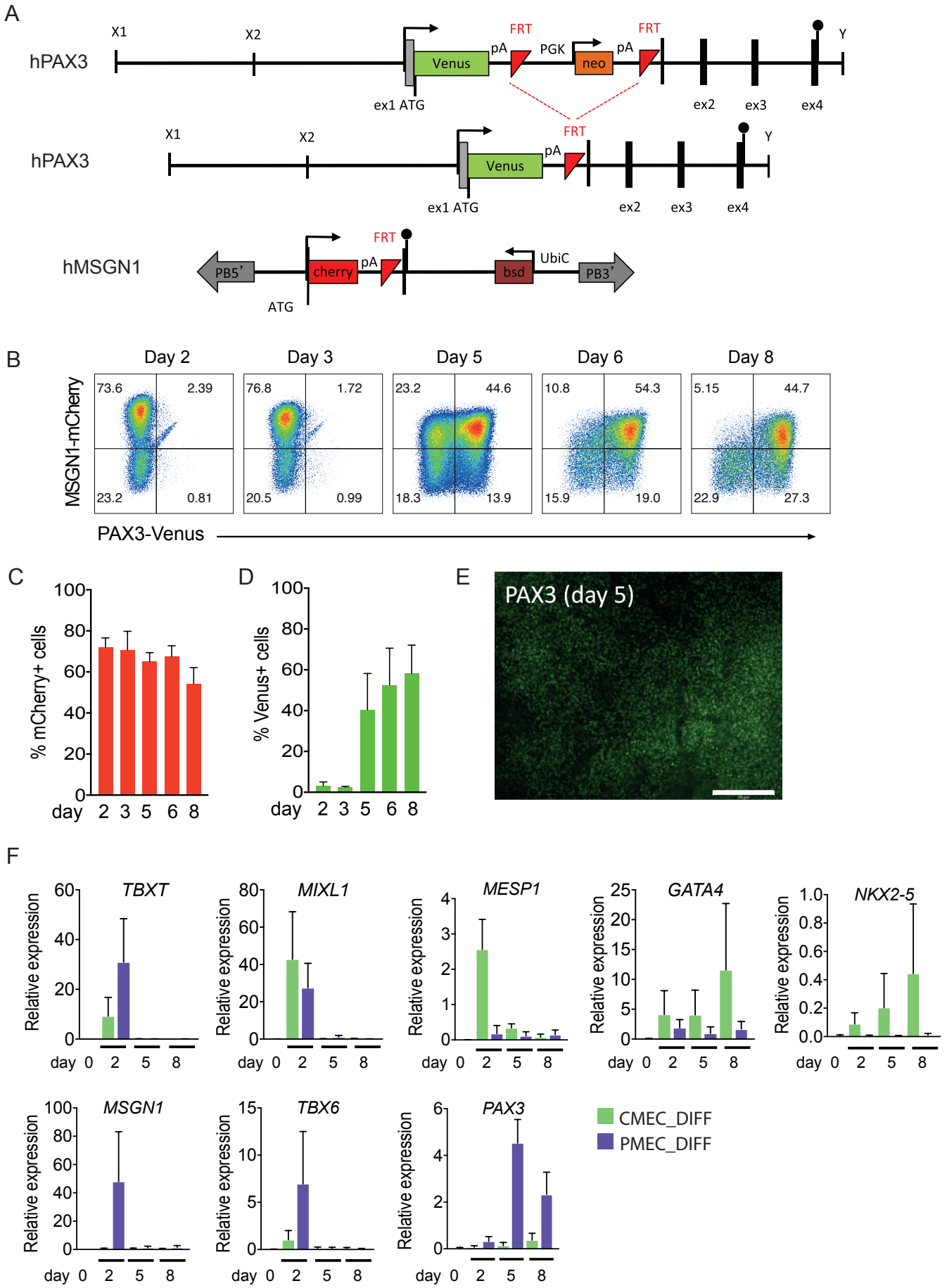
A
hPAX3
X1
X2
Venus
pA
FRT
PGK
neo
pA
FRT
Y
ex1 ATG
ex2
ex3
ex4
hPAX3
X1
X2
Venus
pA
FRT
Y
ex1 ATG
ex2
ex3
ex4
hMSGN1
PB5'
cherry
pA
FRT
ATG
bsd
UbiC
PB3'
B
Day 2
Day 3
Day 5
Day 6
Day 8
MSGN1-mCherry
73.6
2.39
23.2
0.81
76.8
1.72
20.5
0.99
23.2
44.6
18.3
13.9
10.8
54.3
15.9
19.0
5.15
44.7
22.9
27.3
PAX3-Venus
C
% mCherry+ cells
day 2 3 5 6 8
D
% Venus+ cells
day 2 3 5 6 8
E
PAX3 (day 5)
F
TBXT
MIXL1
MESP1
GATA4
NKX2-5
MSGN1
TBX6
PAX3
Relative expression
day 0 2 5 8
CMEC_DIFF
PMEC_DIFF

Figure S2.

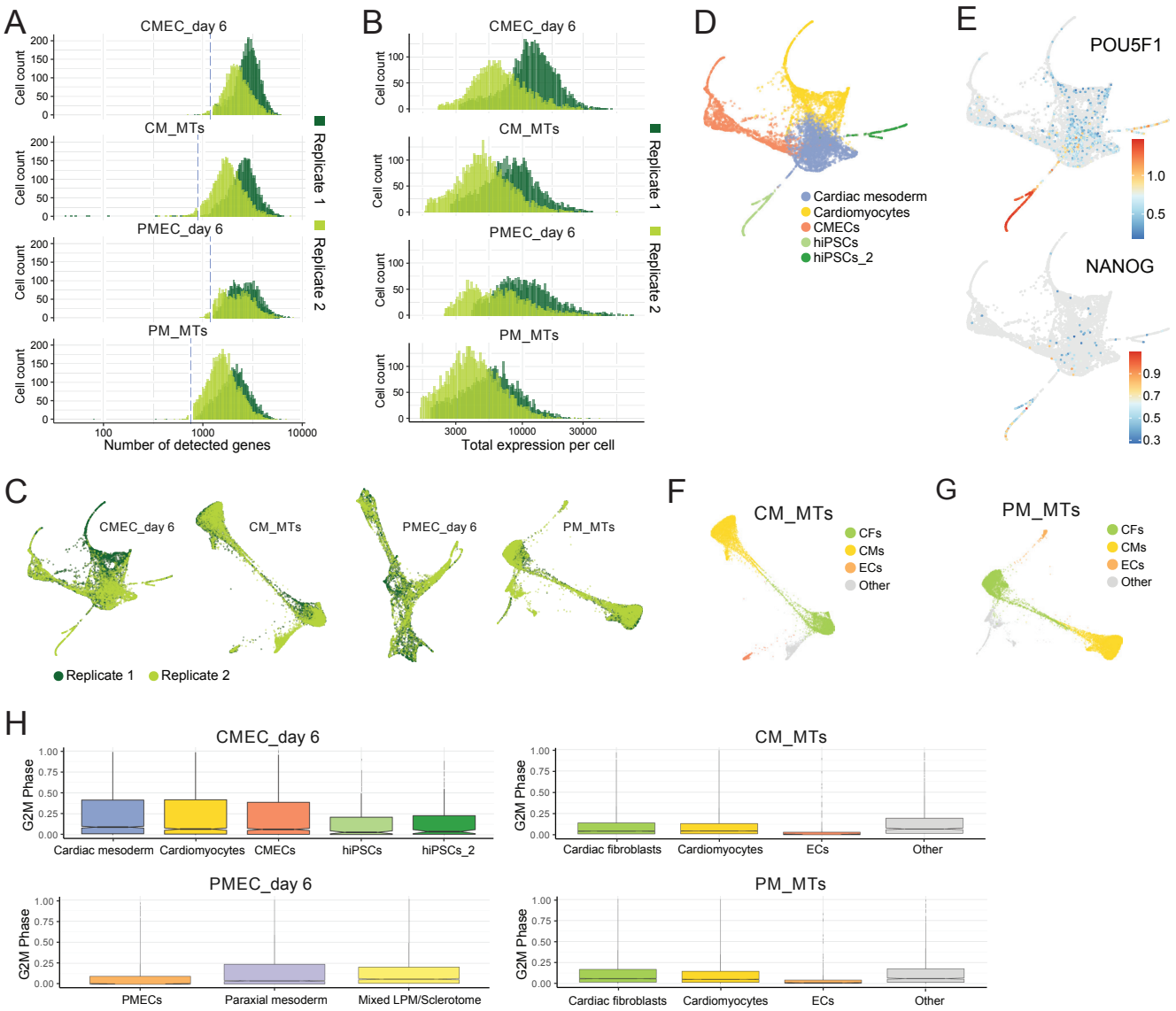
A
CMEC_day 6
CM_MTs
PMEC_day 6
PM_MTs
Cell count
Number of detected genes
Replicate 1
Replicate 2
B
Total expression per cell
C
Replicate 1
Replicate 2
D
Cardiac mesoderm
Cardiomyocytes
CMECs
hiPSCs
hiPSCs_2
E
POU5F1
NANOG
F
CFs
CMs
ECs
Other
G
H
G2M Phase
Cardiac mesoderm
Cardiomyocytes
CMECs
hiPSCs
hiPSCs_2
Cardiac fibroblasts
ECs
PMECs
Paraxial mesoderm
Mixed LPM/Sclerotome

Figure S3.

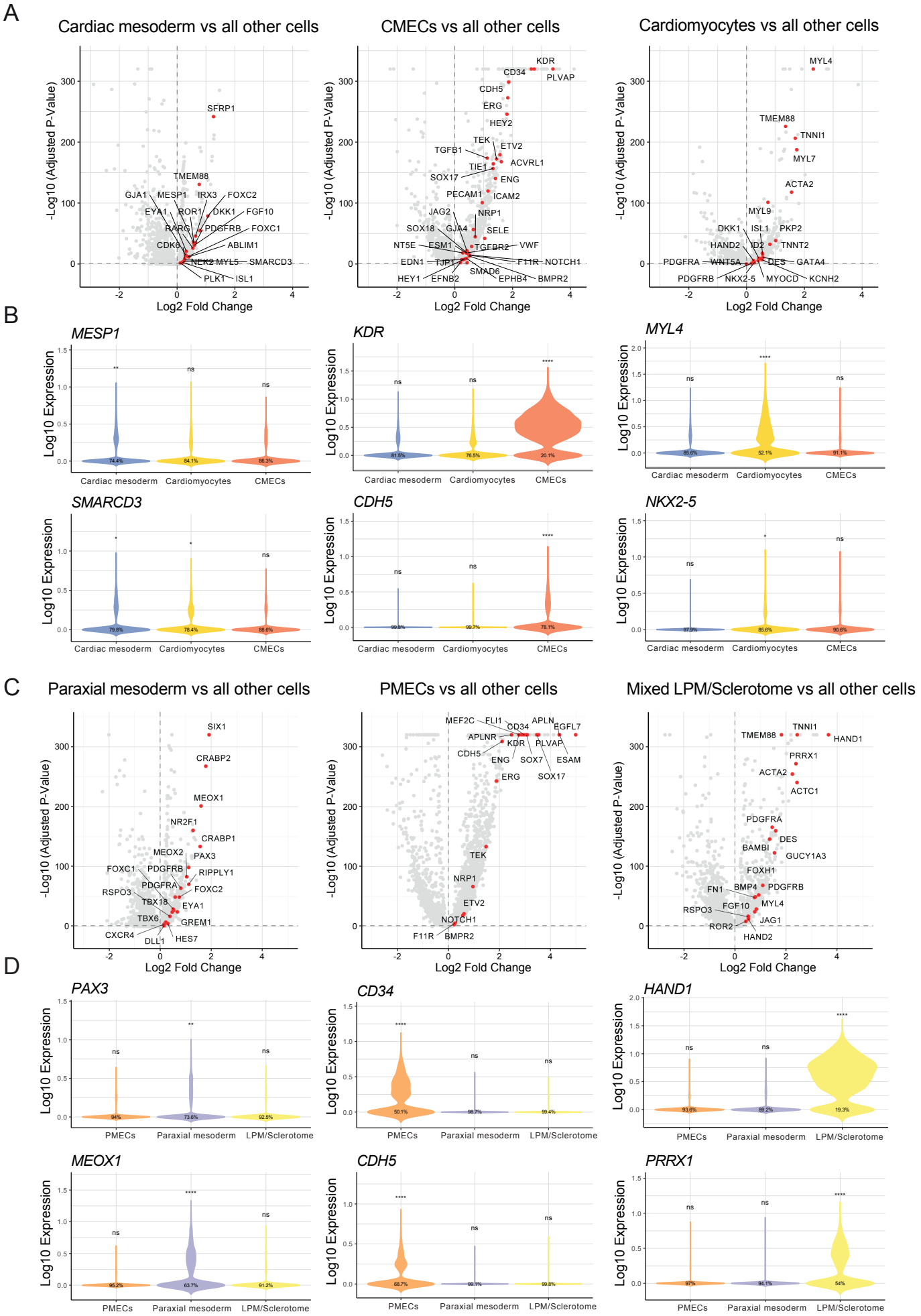
A
Cardiac mesoderm vs all other cells
CMECs vs all other cells
Cardiomyocytes vs all other cells
-Log10 (Adjusted P-Value)
Log2 Fold Change
SFRP1
TMEM88
GJA1
MESP1
IRX3
FOXC2
EYA1
ROR1
DKK1
FGF10
RARG
PDGFRB
FOXC1
ABLIM1
CDK6
NEK2
MYL5
SMARCD3
PLK1
ISL1
KDR
CD34
PLVAP
CDH5
ERG
HEY2
TEK
ETV2
TGFB1
ACVRL1
TIE1
SOX17
ENG
PECAM1
ICAM2
JAG2
NRP1
SOX18
GJA4
SELE
NT5E
ESM1
TGFBR2
VWF
EDN1
TJP1
F11R
NOTCH1
SMAD6
HEY1
EFNB2
EPHB4
BMPR2
MYL4
TNNI1
MYL7
ACTA2
MYL9
DKK1
ISL1
PKP2
HAND2
ID2
TNNT2
PDGFRA
WNT5A
DES
GATA4
PDGFRB
NKX2-5
MYOCD
KCNH2
B
MESP1
KDR
MYL4
SMARCD3
CDH5
NKX2-5
Log10 Expression
Cardiac mesoderm
Cardiomyocytes
CMECs
C
Paraxial mesoderm vs all other cells
PMECs vs all other cells
Mixed LPM/Sclerotome vs all other cells
SIX1
CRABP2
MEOX1
NR2F1
CRABP1
MEOX2
PAX3
FOXC1
PDGFRB
RIPPLY1
PDGFRA
FOXC2
RSPO3
TBX18
EYA1
TBX6
GREM1
CXCR4
DLL1
HES7
MEF2C
FLI1
CD34
APLN
EGFL7
APLNR
KDR
PLVAP
CDH5
ENG
SOX7
ESAM
ERG
SOX17
TEK
NRP1
ETV2
NOTCH1
F11R
BMPR2
TNNI1
TMEM88
HAND1
PRRX1
ACTA2
ACTC1
PDGFRA
DES
BAMBI
GUCY1A3
FOXH1
FN1
BMP4
PDGFRB
FGF10
MYL4
RSPO3
JAG1
ROR2
HAND2
D
PAX3
CD34
HAND1
MEOX1
CDH5
PRRX1
PMECs
Paraxial mesoderm
LPM/Sclerotome

Figure S4.

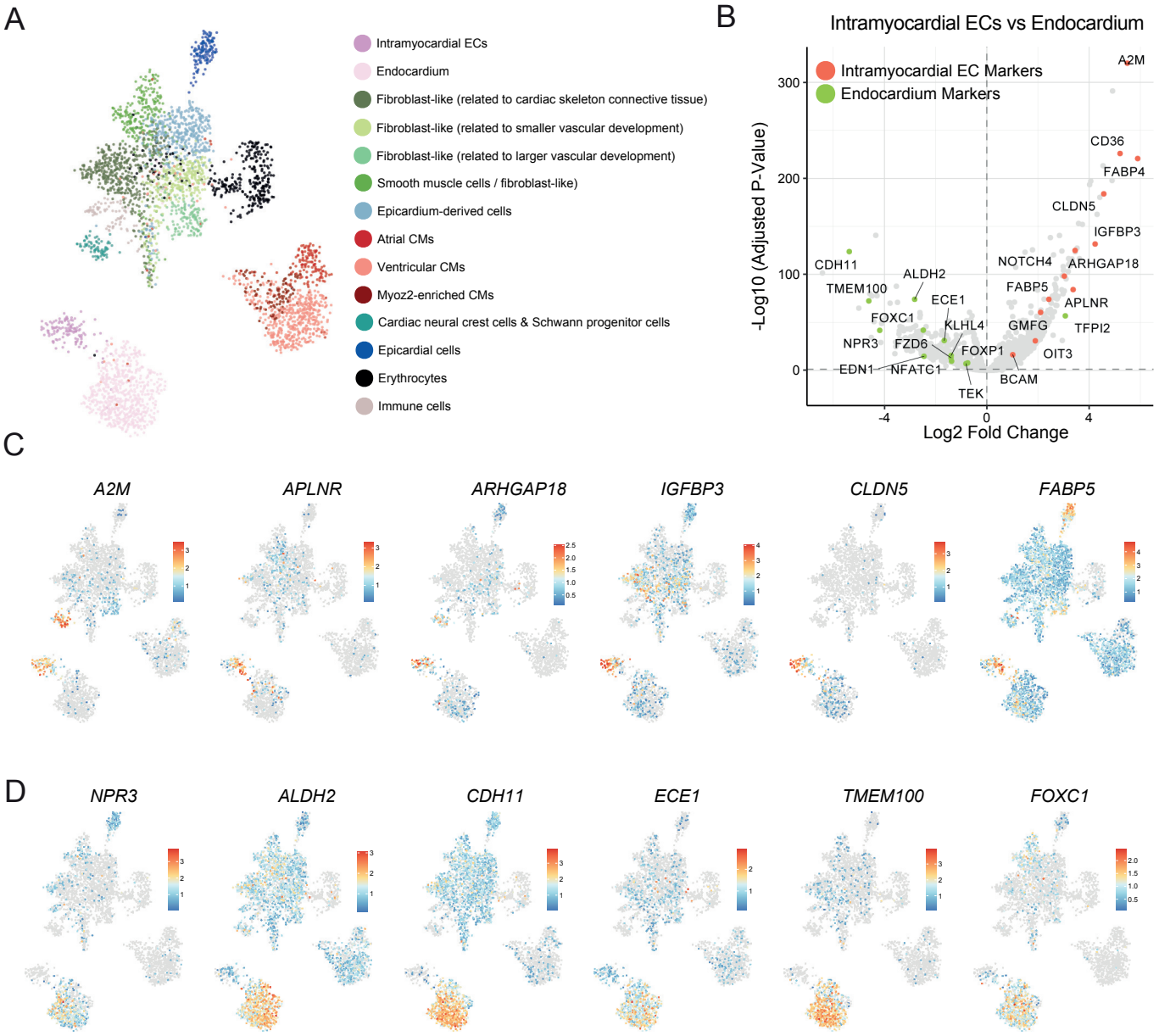
A
Intramyocardial ECs
Endocardium
Fibroblast-like (related to cardiac skeleton connective tissue)
Fibroblast-like (related to smaller vascular development)
Fibroblast-like (related to larger vascular development)
Smooth muscle cells / fibroblast-like)
Epicardium-derived cells
Atrial CMs
Ventricular CMs
Myoz2-enriched CMs
Cardiac neural crest cells & Schwann progenitor cells
Epicardial cells
Erythrocytes
Immune cells
B
Intramyocardial ECs vs Endocardium
Intramyocardial EC Markers
Endocardium Markers
-Log10 (Adjusted P-Value)
Log2 Fold Change
A2M
CD36
FABP4
CLDN5
IGFBP3
NOTCH4
ARHGAP18
FABP5
APLNR
TFPI2
GMFG
OIT3
BCAM
CDH11
ALDH2
TMEM100
ECE1
FOXC1
KLHL4
NPR3
FZD6
FOXP1
EDN1
NFATC1
TEK
C
A2M
APLNR
ARHGAP18
IGFBP3
CLDN5
FABP5
D
NPR3
ALDH2
CDH11
ECE1
TMEM100
FOXC1

Figure S5.

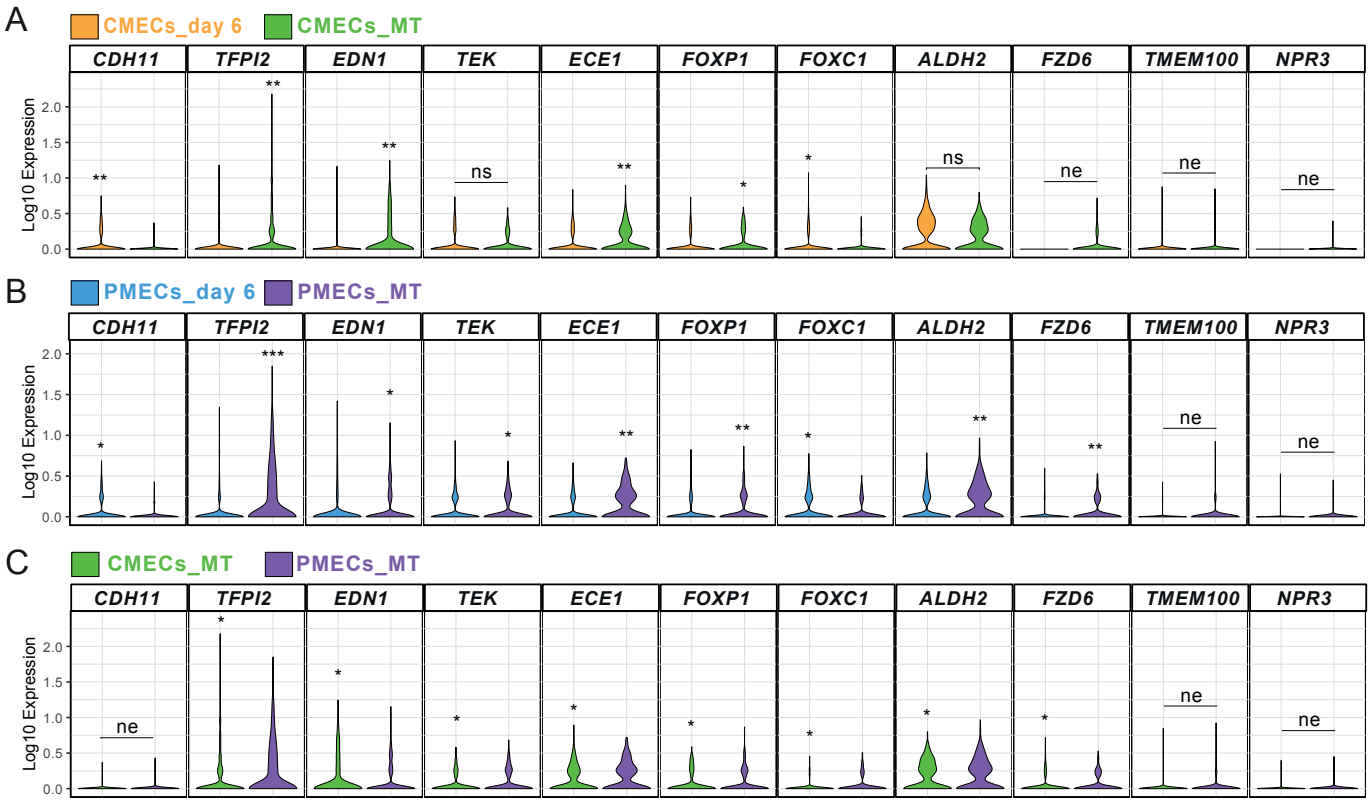
A
CMECs_day 6
CMECs_MT
CDH11
TFPI2
EDN1
TEK
ECE1
FOXP1
FOXC1
ALDH2
FZD6
TMEM100
NPR3
Log10 Expression
2.0
1.5
1.0
0.5
0.0
**
**
**
ns
**
*
*
ns
ne
ne
ne
B
PMECs_day 6
PMECs_MT
CDH11
TFPI2
EDN1
TEK
ECE1
FOXP1
FOXC1
ALDH2
FZD6
TMEM100
NPR3
Log10 Expression
2.0
1.5
1.0
0.5
0.0
*
***
*
*
**
**
*
**
**
ne
ne
C
CMECs_MT
PMECs_MT
CDH11
TFPI2
EDN1
TEK
ECE1
FOXP1
FOXC1
ALDH2
FZD6
TMEM100
NPR3
Log10 Expression
2.0
1.5
1.0
0.5
0.0
ne
*
*
*
*
*
*
*
*
ne
ne